COURSE 6

TRANSPORT THEORY OF MESOSCOPIC SYSTEMS: APPLICATION TO BALLISTIC TRANSPORT

A. Douglas Stone

Yale University, Department of Applied Physics
P.O Box 208284, New Haven, CT 06520, USA

E. Akkermans, G. Montambaux, J.-L. Pichard and J. Zinn-Justin, eds.
Les Houches, Session LXI, 1994
Physique Quantique Mésoscopique
Mesoscopic Quantum Physics

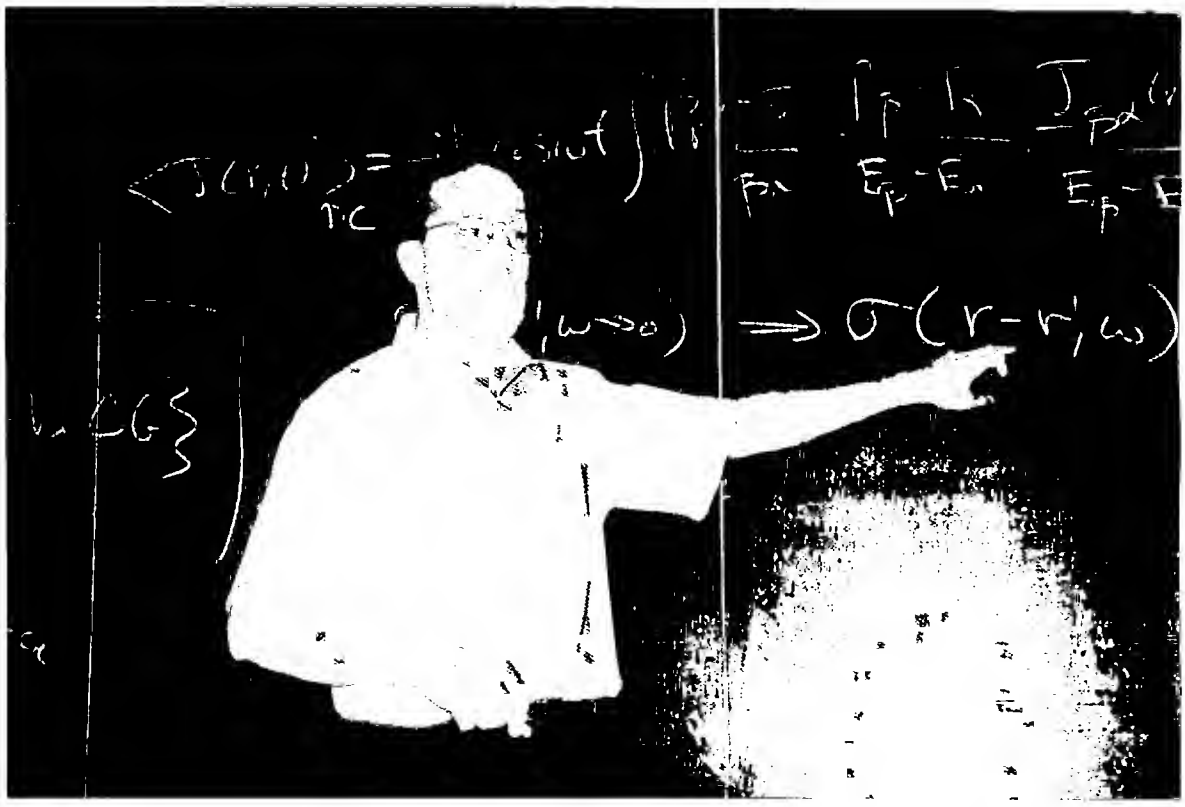

Contents

1. Introduction

1.1. Background

The theory of electronic transport in macroscopic normal metals has traditionally employed the Boltzmann or quasiclassical approach to determine an electronic distribution function in the presence of impurity and phonon scattering, electric and magnetic fields, and band-structure effects [1]. From this distribution function the spatially-averaged current is calculated and conductivity. Hall conductivity and non-linear I–V characteristics are obtained. Successive scatterings are treated as independent and results are averaged over configurations of impurities. Sample geometry is normally not considered relevant as the macroscopic conductivity is an intensive quantity.

Beginning with the prediction and discovery of the weak localization effect in metals [2–4] it was appreciated that at sufficiently low temperatures even in macroscopic conductors the assumption of independent scatterings misses qualitatively new effects related to electronic phase-coherence. However with the discovery of the hc/e period Aharonov–Bohm effect in single metal rings [5,6] and reproducible mesoscopic conductance fluctuations [7–14] it became clear that transport in conductors on the size scale of a micron or below would exhibit properties very different from those of macroscopic conductors. As the physics of these systems became better understood it was recognized that these properties are not characteristic of a fixed size scale but rather depend on the temperature, T, fermi wavelength, k_f and degree of disorder in the material. None of the phenomena discussed in this volume occur in micron-size conductors at room temperature; conversely mesoscopic phenomena such as conductance fluctuations have been observed in conductors of size up to 100 microns at milliKelvin temperatures in samples of high purity and small k_f. Hence the term *mesoscopic* was introduced to denote a physical regime for transport and not a specific size scale.

1.2. Novel properties of mesoscopic conductors

The novel transport properties of mesoscopic conductors may be roughly summarized as follows:

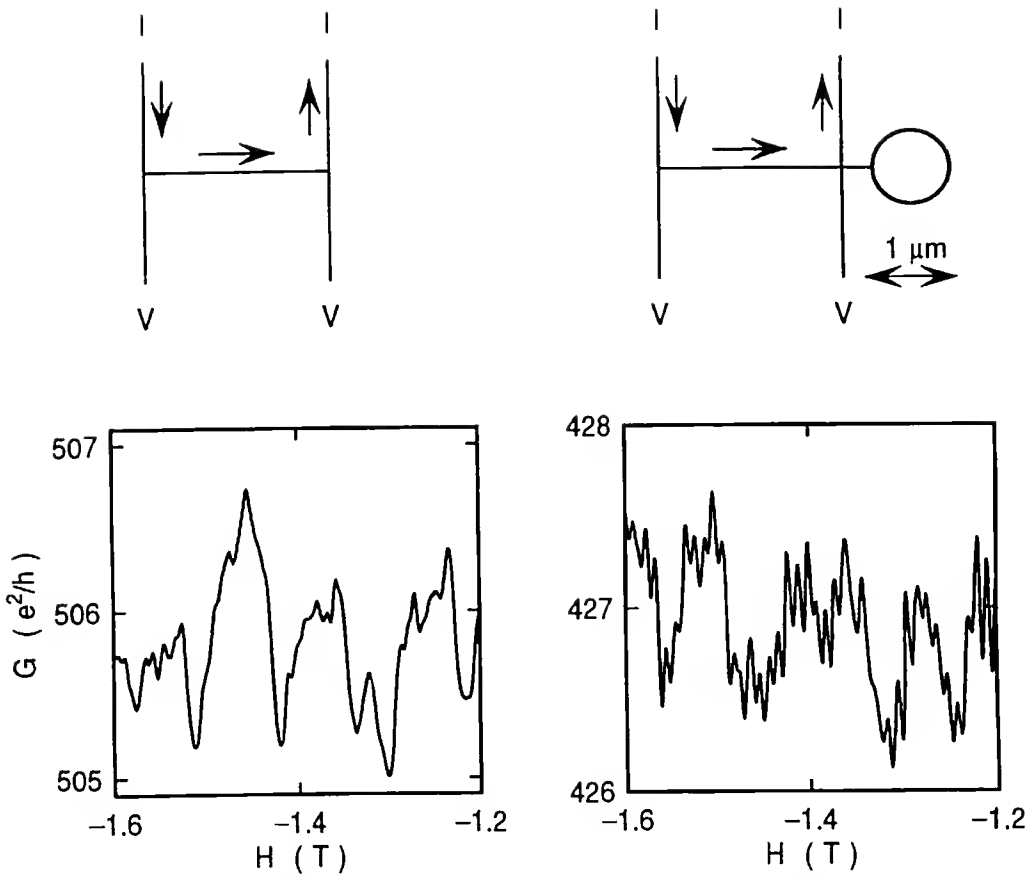

Fig. 1. Measurement of non-local Aharonov–Bohm oscillations in conductance by Umbach et al. [17]. For sample with loop attached outside the current path the periodic A–B oscillations are superimposed on the aperiodic universal conductance fluctuations. Adapted from [18].

Sample-specificity. Mesoscopic conductors of the same material fabricated in the same manner will have different measured transport coefficients. This is illustrated by the different (but reproducible) conductance fluctuations as a function of magnetic field (or other external parameters) measured in mesoscopic samples (see Fig. 1).

Non-locality. The measured transport properties of a mesoscopic conductor do not depend solely on the portion of the sample between the measuring points. If the phase-coherence length [15,16] is sufficiently large then regions of the sample outside the current path strongly influence the measured properties.

This is illustrated dramatically by the experimental data shown in Fig. 1 [17]. In this experiment a mesoscopic ring was attached to a conducting microstructure outside the current path and was found to a yield a measurable hc/e Aharonov–Bohm oscillation in the magnetoresistance due to the interference between electronic trajectories along the main current path and those which detour around the ring.

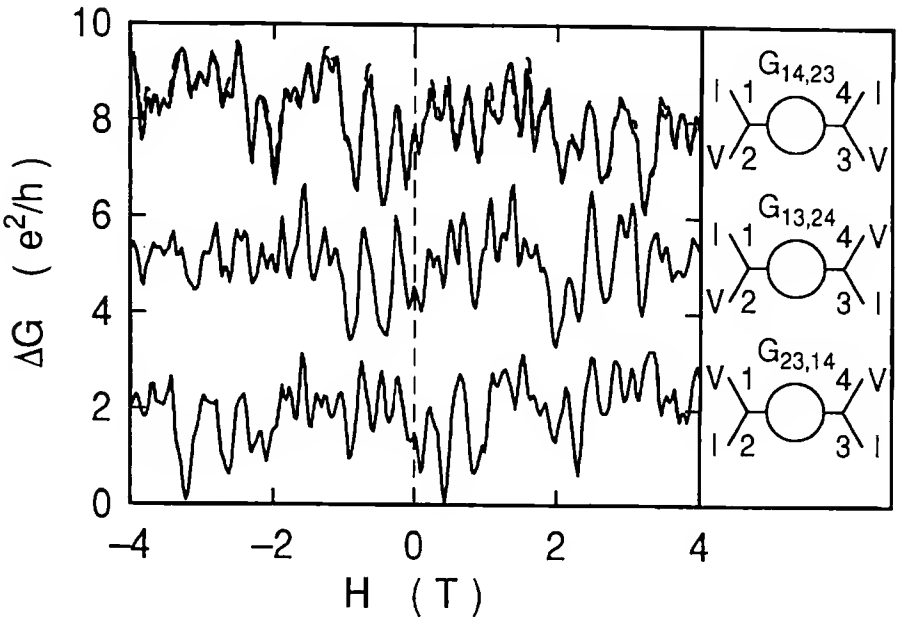

Fig. 2. Magnetoconductance measurements taken for three different configurations of current and voltage leads. The AB oscillations have been filtered out of the data. Note the complete lack of symmetry around $B = 0$ for a given measurement, but the mirror symmetry of the top and bottom traces. This symmetry is required by reciprocity relations to be discussed below. Reprinted from [6].

Violation of macroscopic symmetries. A number of symmetries found in the properties of macroscopic conductors are violated by mesoscopic conductors [11]. These are symmetry properties that do not follow immediately from microscopic symmetries but also require further conditions (e.g. symmetry of the scattering potentials on average) which were often not explicitly recognized until they were found to be violated in mesoscopic conductors. One striking example is the longitudinal magnetoresistance. A standard measurement of R_{xx} involves injecting and collecting a current at two ends of the sample and measuring the voltage induced between additional probes attached along the sample with the second voltage probe displaced a distance much larger than the width of the wire. Under these conditions in a homogeneous macroscopic conductor the Hall contribution to the measured resistance is negligible and one measures a magnetoresistance which is symmetric in B. However this symmetry does not follow from the fundamental Onsager symmetries of the non-local resistivity tensor (see below): it also relies on approximate symmetries of the transmission probabilities for electrons which are violated in the mesoscopic regime. In fact it has been shown [20,19,21] that no matter how one attaches the voltage probes in a phase-coherent sample the fluctuating part of the measured resistance arises roughly equally from the symmetric ("longitudinal") and anti-symmetric ("Hall") resistivities so that the resulting magnetoresistance has no symmetry under field reversal (see Fig. 2). Similarly the I–V characteristic in mesoscopic samples becomes asymmetric at

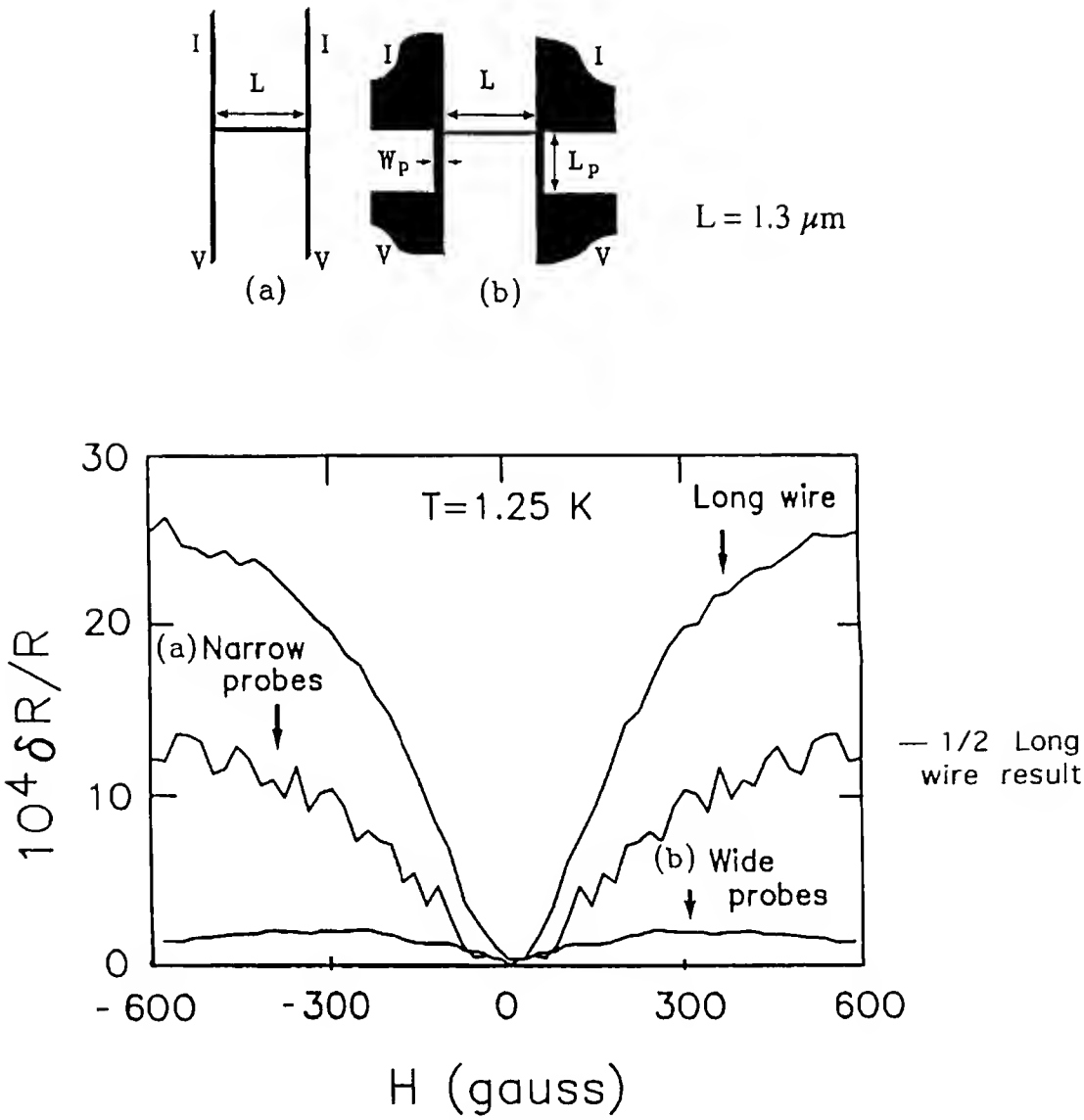

Fig. 3. Weak localization effect in 3 cases: Top trace is a wire much longer than the phase coherence length. Middle and bottom traces are from similar mesoscopic wires attached to narrow and wide probes respectively. Reprinted from [23].

extremely small voltages corresponding to internal electric fields much smaller than are needed to observe non-linearities in conventional conductors [22].

Dependence on measurement geometry. Measured resistances also depend on what type of probes are employed. In Fig. 3 is shown a comparison [23] of weak localization magnetoresistance for two mesoscopic samples which differ primarily in the nature of the voltage and current probes used. The sample with narrow probes shows a WL amplitude roughly one order of magnitude larger than the comparable sample with wide probes. Intuitively this is related to the difficulty an electron has in returning phase-coherently to the sample from the wide leads.

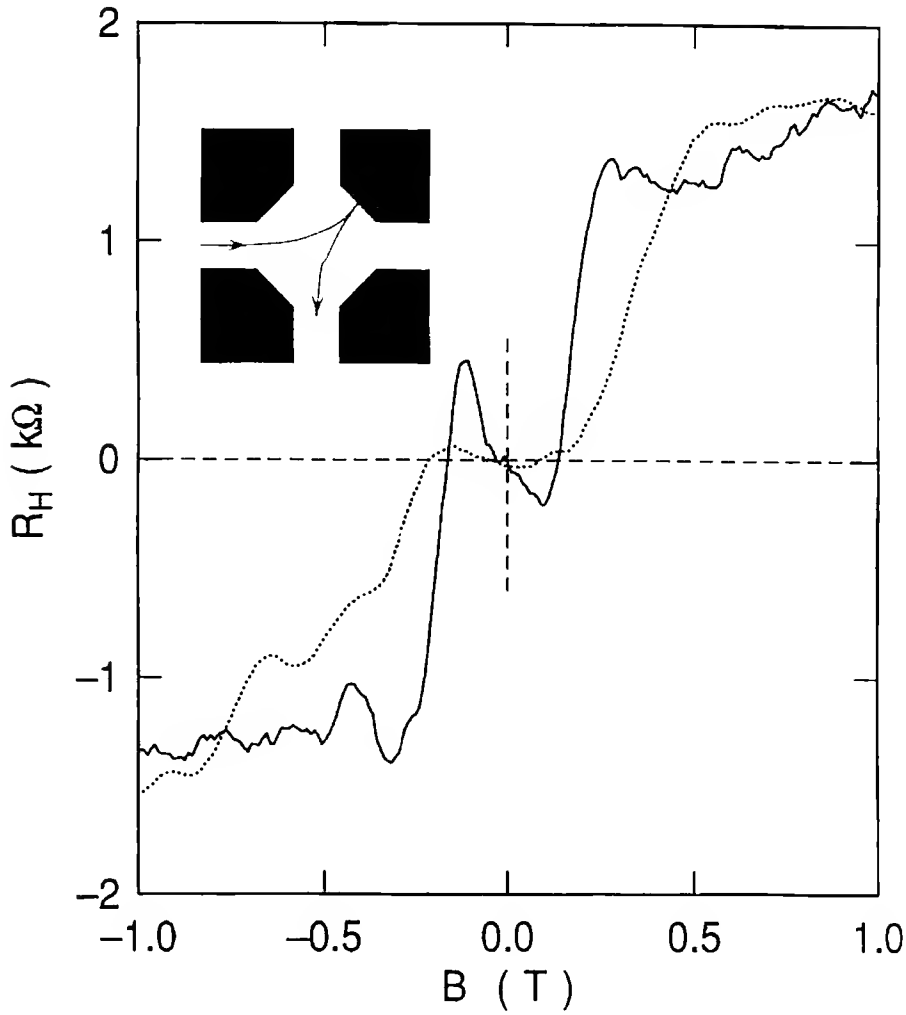

Fig. 4. Hall resistance of a GaAs quantum wire junction with flattened corners (inset) which leads to inverted Hall resistance (solid line); data from a nominally square-cornered junction (dashed line) show quenching (vanishing slope near $B = 0$) but not inversion. Inset shows classical rebound mechanism for quenching and inversion discussed in section 4.4. Adapted from [24].

Dependence on sample geometry. Much of this chapter will focus on extremely high-mobility semiconductor microstructures (as opposed to disordered metallic conductors which are treated in detail in chapter [15,16]). In the high-mobility microstructures the dominant source of resistance is the sample geometry itself. This is illustrated in Fig. 4 where we show Hall resistance data [24] from GaAs quantum wire junctions with differing geometries.

These results taken together demonstrate that the concept of resistivity as an intensive quantity breaks down at the mesoscopic scale. Instead one needs to develop a transport theory based on sample-specific quantities: i.e. quantities which are meaningful for a given sample measured in a given manner. We now review the main approaches which have been developed to describe mesoscopic transport.

2. Sample-specific theory

2.1. Conductance coefficients

A typical mesoscopic transport measurement is performed by imposing a very low frequency AC current through the microstructure and measuring the voltages induced between various auxiliary probes (this is called a multiprobe resistance measurement). At sufficiently small currents there must be a linear relationship of the form

$$I_m = \sum_{n=1}^{N_L} g_{mn}(V_n - V_0), \tag{2.1}$$

where I_m is the current measured in probe m and $V_n - V_0$ is the difference between the voltage measured at probe n and a reference voltage V_0. The g_{mn} are the *conductance coefficients* and are independent of voltage at small currents. In a typical measurement a current I is injected in a given probe (probe 1) and extracted through probe 2 and the other "voltage probes" draw no current; hence Eq. (2.1) is to be solved with $I_1 = I, I_2 = -I, I_m = 0, m = 3, 4, \ldots$. The resistances are given by $R_{12,mn} = (V_m - V_n)/I$, where the first pair of indices denote the current leads and the second the voltage leads. Since the resistances must be independent of the reference voltage V_0 and the currents must satisfy Kirchhoff's law ($\sum_{m=1}^{N_L} I_m = 0$) the conductance matrix g must satisfy $\sum_{m=1}^{N_L} g_{mn} = \sum_{n=1}^{N_L} g_{mn} = 0$. These two conditions are independent in general as g need not be symmetric (we shall find it is symmetric only in the absence of a magnetic field). These conditions imply that g is only invertible in the subspace perpendicular to the vector $(1, 1, 1, \ldots)$ and solutions of Eq. (2.1) have a non-uniqueness corresponding to the redefinition of zero voltage. The conductance matrix g contains in principle all the sample-specific information relating to the linear resistance of mesoscopic conductors. The challenge then is to calculate the g_{mn} in a manner which includes the effects of phase-coherence and sample and measuring geometry which we have seen above are important. The main approach to meeting this challenge has been to relate the conductance coefficients to an appropriate quantum-mechanical scattering problem. This was achieved by arguments due to Landauer, Imry and Büttiker; it has also now been understood that the same conclusion can be reached by applying quantum linear response theory.

2.2. The scattering approach

I will not provide a full historical review of the literature on this topic here, as I have done so elsewhere [25]. Briefly, long before the birth of mesoscopic phys-

ics Rolf Landauer [26] gave a physical argument leading to the conclusion that a truly one-dimensional phase-coherent quantum-mechanical conductor should have a conductance given by $g = (e^2/h)T/R$, where T, R referred to the total transmission and reflection coefficients of the conductor(I will neglect spin except when needed for comparison with experiment). This formula had the intuitively appealing property that as the sample transparency approached unity ($T \rightarrow 1$) its resistance vanished. The first attempts to derive this formula from linear response theory however yielded the result $g = (e^2/h)T$ [27] or its many-channel generalization [28] $g = (e^2/h)\sum_{a,b=1}^{N_c} T_{ab}$, where a, b index the N_c channels injecting from the leads. Engquist and Anderson [29] showed quite early that the Landauer formula really was meant to describe a four-probe measurement and Imry [30] subsequently understood that $g = (e^2/h)T$ described an ideal two-probe measurement. He pointed out that the non-vanishing resistance predicted by this formula for a "perfect conductor" ($T \rightarrow 1$) actually represents an ideal quantum contact resistance which is unavoidable in a two-probe configuration. Very shortly thereafter this quantized contact resistance was directly observed in semiconductor point contacts in GaAs heterostructures [31,32]. Büttiker [33,34] completed the development of the scattering approach by focusing on the entire conductance matrix and showing that a generalization of Landauer's original "counting argument" leads to a simple and useful theory for the quantum conductance matrix with the correct time-reversal symmetry properties. I now reproduce this argument.

The sample whose resistances are being measured is assumed to be attached to N_L perfect phase-randomizing reservoirs all at chemical potential μ_0 through ideal leads which can serve either as current or voltage probes. When voltages or currents are imposed between the reservoirs (which roughly correspond to massive contacts in real experiments) in general current will flow transiently into or out of all the reservoirs. However the chemical potentials of those reservoirs chosen to be voltage probes will be adjusted until these currents are cancelled, leaving a steady-state voltage V_n on all the probes. Denote the current into probe m due to the voltage (measured from equilibrium) on probe n as I_{mn} where $I_m = \sum_{n=1}^{N_L} I_{mn}$. Assuming $m \neq n$ we can write $I_{mn} = \sum_{b=1}^{N_c} I_{nb}^0 \sum_{a=1}^{N_c} T_{mn,ab}$, where I_{nb}^0 is the current injected in channel b from probe n in the energy interval $eV_n - \mu_0$ and $T_{mn,ab}$ is the transmission coefficient from lead n, channel b to lead m, channel a. Since the reservoirs are assumed to feed each incident channel equally, the current $I_{nb}^0 = ev_b(dn_b^+/d\epsilon)eV_n$ where v_b is the velocity in channel b and $dn_b^+/d\epsilon$ is the density of ingoing states in channel b in lead n (we assume all leads have the same channel states for simplicity; this assumption is not required). If one imagines the lead to be perfectly translationally invariant in the longitudinal direction then one has the equality $v_b dn_b^+/d\epsilon = 1/2\pi\hbar = 1/h$. This identity

holds for non-interacting quantum particles with arbitrary transverse confinement in the presence of a uniform magnetic field of arbitrary strength. The translational invariance in the longitudinal direction means that the propagating states may be labelled by a wavevector k and a mode index b such that their longitudinal velocity is $\hbar v_b = d\epsilon_b(k)/dk = (2\pi dn_b^+/d\epsilon)^{-1}$. Because this only holds for non-interacting particles the scattering approach only holds for quasi-particles which carry unit charge as in fermi liquids and must be non-trivially generalized to treat mesoscopic superconductors or the fractional quantum Hall regime. Combining these results yields

$$I_m = \sum_{n=1}^{N_L} I_{mn} = \frac{e^2}{h} \sum_{n=1}^{N_L} (T_{mn} - N_c \delta_{mn}) V_n \equiv \sum_{n=1}^{N_L} g_{mn} V_n \tag{2.2}$$

(the term $N_c\delta_{mn}$ arises when the argument is applied to the case $m = n$ and we have set $V_0 = 0$). Here

$$T_{mn} = \sum_{a,b=1}^{N_c} T_{mn,ab} = \mathrm{Tr}\{t_{mn} t_{mn}^\dagger\}, \tag{2.3}$$

where t_{mn} is the transmission amplitude matrix between the channel states and t_{mm} is to be interpreted at the reflection matrix. One can easily see that the unitarity relations for the S-matrix ensure that Eq. (2.2) is consistent with the conditions on the conductance matrix $\sum_{m=1}^{N_L} g_{mn} = \sum_{n=1}^{N_L} g_{mn} = 0$ and do not alone require that $\mathbf{g}$ be symmetric.

2.3. *Time-reversal symmetry constraints on* $\mathbf{g}$

Since Eq. (2.2) directly relates the g_{mn} to a current-conserving quantum S-matrix, it is straightforward to find the constraints time-reversal (TR) symmetry imposes on the $g_{mn}(B)$ and hence the magnetoresistances. $\mathbf{S}$ relates the two N_cN_L-dimensional vectors of incident and outgoing fluxes, $\boldsymbol{I}, \boldsymbol{O}$: $\mathbf{S}(B)\boldsymbol{I} = \boldsymbol{O}$. Neglecting spin, TR symmetry implies that if the magnetic field is reversed then initial and final states may be interchanged (as long as they are complex conjugated): $\mathbf{S}(-B)\boldsymbol{O}^* = \boldsymbol{I}^*$. Using the unitarity of the S-matrix this equation implies

$$\mathbf{S}^T(-B) = \mathbf{S}(B). \tag{2.4}$$

When $B = 0$ this immediately implies that $\mathbf{g}$ is a symmetric matrix. An important case is if the conductor is only attached to two-probes, so that the conductance matrix is only 2×2. Then the requirements that its rows and columns add up to zero imply that the matrix is always symmetric, independent of the presence of a magnetic field; hence that $g_{12} = g_{21} \equiv g$ is symmetric in magnetic field. In fact

two-probe measurements of mesoscopic conductance fluctuations do find that the complicated sample-specific magnetofingerprint is symmetric in B.

In the general multiprobe case the conductance formula (2.2) and time-reversal symmetry of the S-matrix only imply the following symmetry:

$$g_{mn}(B) = g_{nm}(-B). \tag{2.5}$$

This relation does *not* imply any symmetry between a single resistance measurement at positive and negative fields. The symmetry under field reversal observed in standard longitudinal magnetoresistance measurements (and antisymmetry in Hall measurements) arises because the impurity potentials involved are macroscopically homogeneous (the violation of these symmetries in macroscopically inhomogeneous conductors was known previously [35]). Although these symmetries are often referred to as Onsager relations we shall see that it is only the Onsager relation for the non-local conductivity (and the reciprocity symmetry to be discussed immediately below) which follows from TR symmetry alone. In mesoscopic transport, where quantum interference effects are known to be extremely sensitive to the details of the impurity potential or sample geometry, typically the spatial potentials or the measuring configuration has some asymmetry and one observes significantly asymmetric magnetoconducance as seen in Fig. 2. However Eq. (2.5) does imply an experimentally verifiable reciprocity relation [34]:

$$R_{mn,m'n'}(B) = R_{m'n',mn}(-B). \tag{2.6}$$

Hence the same resistance is obtained from two different measurements: in the first measurement current is run from lead m to n and voltage measured between m', n' at field B; in the second measurement current and voltage leads are interchanged and the field is reversed. The validity of Eq. (2.6) can be seen by the following argument. As noted in section 2.1 above, although $\mathbf{g}$ is not invertible in general, it is invertible in the physical subspace of vectors satisfying Kirchhoff's Laws. Denote the inverse $\mathbf{r}$, and define unit vectors $\hat{e}_n, n = 1, 2, \ldots N_L$ corresponding to unit current (or voltage) on each probe. It follows then from $I = \mathbf{g}V$ that the resistance $R_{mn,m'n'}(B) = (\hat{e}_{m'} - \hat{e}_{n'}) \cdot \mathbf{r} \cdot (\hat{e}_m - \hat{e}_n)$. $R_{m'n',mn}(-B)$ is the transpose of this with $\mathbf{r}(B) \rightarrow \mathbf{r}(-B)$. But this is just equal to $R_{mn,m'n'}(B)$ as long as $\mathbf{r}$ satisfies $\mathbf{r}^T(-B) = \mathbf{r}(B)$ which is straightforward to confirm from Eq. (2.5).

2.4. Resistance quantization and negative resistance

As noted above, the general properties of the conductance matrix $\mathbf{g}$ and hence of the resistances $R_{m'n',mn}$ follow from Kirchoff's laws and time-reversal symmetry. The reciprocity symmetry Eq. (2.6) was known previously and derived

under classical assumptions of a local conductivity obeying Onsager's relations [35]. (Büttiker's argument shows that they hold even in the mesoscopic regime when a local conductivity cannot be defined.) The basic novelty of the scattering approach (as compared e.g. with quasiclassical transport) is the explicit appearance of the quantum unit of conductance e^2/h in the conductance matrix. This implies that under conditions in which the transmission probabilities become quantized, the resistances will measure this quantum unit of conductance. Two experimentally realized examples are semiconductor point contacts and quantum Hall resistors. The semiconductor point contacts were created by dividing a GaAs 2DEG with a split gate [31,32]. When negatively charged this gate created a constriction with a width dependent on the magnitude of the gate voltage and a length comparable to the gate width of roughly 2500 Å. In these high-mobility structures the electrons were negligibly back-scattered in traversing the constriction. Thus the structure was similar to the "perfect" conductor connecting two reservoirs (represented by the wide regions of the 2DEG). The transmission coefficients for the propagating channels in the constriction were essentially unity; the number of propagating channels depended on the voltage on the constricting gate leading to conductance jumps of $2e^2/h$ with decreasing (negative) gate voltage every time a new channel began to propagate (see Fig. 5, the factor of two is for spin).

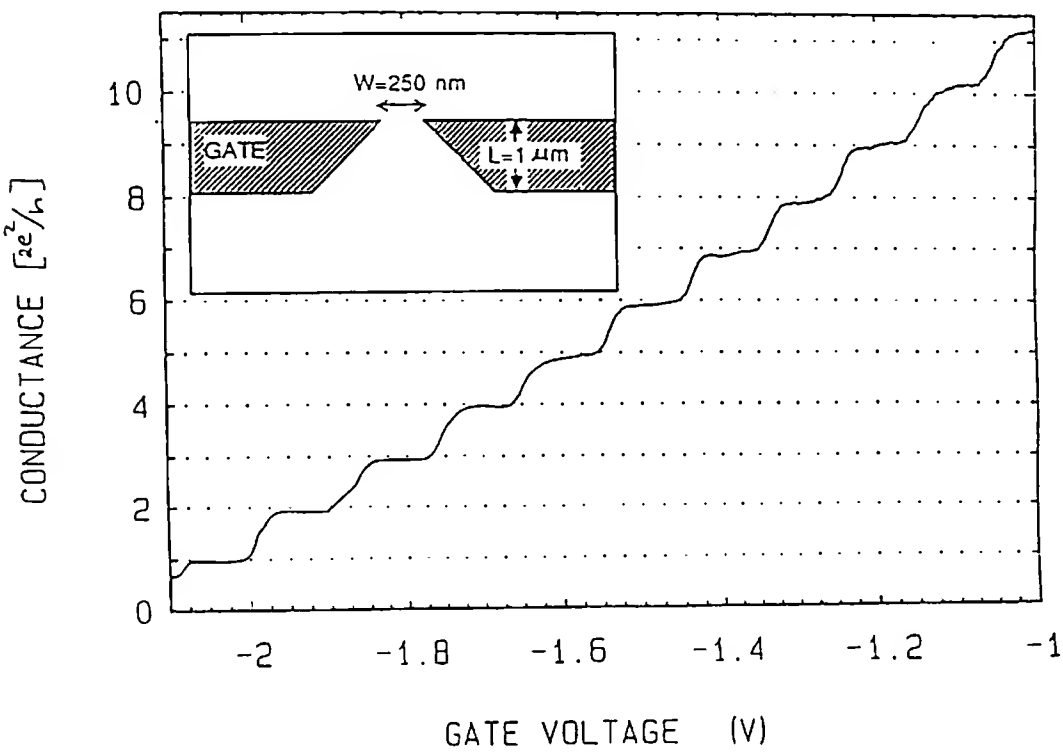

Fig. 5. Conductance of a semiconductor point contact as a function of gate voltage which controls the size of the constriction; inset shows schematic of the structure. Adapted from [31].

Although this effect follows straightforwardly from the two-probe conductance formula $g = (e^2/h)\sum_{a,b}^{N_c} T_{ab}$ if one assumes an ideal connection between the "reservoir" and the "sample", its clear appearance in this experiment was not anticipated since no special effort was made to match adiabatically [36] the wide and narrow regions. Later theoretical work [37] showed that even in the limit of a completely abrupt interface which generates strong inter-channel scattering rather sharp transmission steps occur at $T = 0$.

A second example is the integer quantum Hall effect. This is not a mesoscopic effect and does not require samples small with respect to either the elastic mean free path or the inelastic mean free path. Nonetheless it has been possible to develop a scattering approach to the IQHE in which the channels refer to edge-states at the fermi energy (see section 3.3 below) which yields some insight into the origin of the quantization and some predictions regarding experiments in inhomogeneous geometries [38,40,39]. Space limitations do not allow me to review this literature here.

A final point is that the four-probe resistances obtained from Eq. (2.5) are not a measure of the power dissipated in the sample and are not necessarily positive. The power expended in transfering elctrons from the source to sink is equal to the product IV, but need not be dissipated anywhere in the sample, and in the absence of significant inelastic scattering will all appear in the sink. In contrast to our intuition from macroscopic conductors, any particular four-probe resistance can turn out to be positive or negative (with an absolute value bounded by the two-probe resistance) depending on the details of the particular scattering configuration within the sample. Such negative resistances have actually been measured in microstructures, arising either due to quantum interference effects [41] or due to bends in ballistic microstructures [42,43].

3. Sample-specific linear response theory

3.1. Model hamiltonian for mesoscopic conductors

Equation (2.2), which relates the conductance coefficients of a mesoscopic system to a quantum scattering problem, has proved very useful in the theoretical description of experiments on both disordered and ballistic microstructures. However its derivation involves the concept of an ideal electron reservoir and depends on the assumption that the current is carried by non-interacting fermions [44]. It has therefore been of interest to connect [25] this more heuristic treatment of quantum conductance to conventional quantum linear response theory (LRT) pioneered by Kubo and Greenwood [45]. The latter approach is used in most standard texts (for example, [46]) and is the basic technique for introducing many-body effects into

the theory of the macroscopic transport coefficients. Moreover any actual microscopic calculation using the scattering approach needs to introduce a hamiltonian since transmission coefficients are only defined for an infinite hamiltonian system with an asymptotic region in which scattering is absent. We will now show that there is a well-defined hamiltonian system for which one can derive Eq. (2.2) for the conductance coefficients. From the technical point of view the most interesting aspect of the derivation is that it is valid in arbitrary magnetic field and hence provides a rigorous formulation for calculating microscopically the Hall resistance (to all orders in the magnetic field). Until Büttiker's work [33] no formulation of comparable simplicity was known, and indeed there was confusion in the literature as to whether the Hall resistance could be expressed as a fermi surface property. The derivation presented here is based on that of references [40,47].

Our model consists of a finite region (the "sample") in which there is a uniform magnetic field of arbitrary strength, an arbitrary static potential $U(\boldsymbol{r})$ and (initially) an arbitrary electron–electron interaction $V(\boldsymbol{r}-\boldsymbol{r}')$, connected to N_L infinite "leads" which emanate radially outward from the sample and confine the electrons to non-overlapping spatial channels in the asymptotic region. The leads are "perfect" in the sense that they are translationally invariant in the longitudinal direction and the impurity and interaction potentials are assumed to vanish in the leads. The magnetic field is not assumed to vanish in the leads. Since the system is infinite, solutions to the Schrödinger equation exist at all energies above the threshold for propagation at infinity (which we will take to be the zero of energy). Since the system is described by a hermitian hamiltonian, current and energy are exactly conserved and in the equilibrium state no net current flows through the sample (although for $B \neq 0$ there will be a circulating current giving rise to orbital magnetization). Now we wish to introduce a perturbation which represents the effect of imposing a voltage across the sample. In a real conductor placed between the terminals of a battery, charge carriers are literally injected and collected at the terminals by means of a chemical reaction which causes charge transfer against the local electric field [48]. It is not obvious how to represent such a process in terms of a simple perturbing operator acting on the electrons. However we attempt to mimic the effect of the battery by imposing an external potential $\phi(\boldsymbol{r})\cos\omega t e^{\delta t}$ where $\phi(\boldsymbol{r})$ tends to a fixed set of constants $\{V_n\}, n = 1, 2, \ldots, N_L$ on the leads (and $t < 0$). The external potential must be turned on adiabatically in order to connect it with the equilibrium state in the past [46], hence the perturbation takes the form:

$$V(t) = e \int \rho(\mathbf{r})\,\phi(\mathbf{r})\,\cos\omega t e^{\delta t}\,d\mathbf{r}, \tag{3.1}$$

where ρ is the electron density operator.

Note here that $\phi(r)$ describes the *external* potential and its gradient gives only the external electric field; in the presence of this perturbation there will be an induced charge to linear order in the external potential which (when we include electron–electron interactions) will yield an additional induced potential. Hence the total electric field in the sample differs from $-\nabla\phi$ and the conductivity associated with the total electric field differs from that associated with the external field. Below we will calculate the conductivity and the conductance coefficients associated with the *external field* which may initially appear to yield a physically suspect result. However it must be remembered that the *current* induced by the external field already is linear in the field and can have no correction due to induced charge in linear response (see ref. [44]). So linear current response need only take into account correctly electron–electron interactions *in the equilibrium state*. For example the scattering cross-sections assigned to impurities must take into account self-consistent screening. However the currents are determined by the external potential and the voltages on the leads are fixed by the power supply. Therefore despite the fact that standard texts often state that the conductivity associated with the total field is the only physically-relevant quantity [46], there is no need to calculate this conductivity in order to obtain the linear conductance coefficients.

3.2. Kubo non-local conductivity tensor

General many-body linear response theory [49] gives the induced current due to this perturbation as

$$\mathbf{J}(\mathrm{r},\mathrm{t}) = \frac{-ie}{\hbar}\lim_{\delta\to 0}\int_{-\infty}^{t} dt' e^{\delta t'}\cos\omega t' \int d\mathbf{r}' \left\langle [\mathrm{j}(\mathbf{r},t),\rho(\mathbf{r}',t')]\right\rangle \phi(\mathbf{r}'). \tag{3.2}$$

Here the square brackets denote the commutator and the angle brackets denote the thermal equilibrium quantum expectation values obtained by taking the trace of the operator multiplied by the density matrix of the grand canonical ensemble: $\exp[-\beta\mathbf{K}_0]/Z_G$ where $Z_G = \mathrm{Tr}\{\rho_G\}$ is the grand partition function and $\mathbf{K}_0 = \mathbf{H}_0 - \mu\mathbf{N}$ ($\mathbf{H}_0$ is the unperturbed hamiltonian including electron–electron interactions). The operators are written in the interaction representation and hence are time-dependent. Equation (3.2) expresses the current in terms of ϕ whereas to extract the conductivity tensor we wish to relate the current to the electric field. We can do this using a trick due to Kubo which is described in detail in ref. [46]. The expectation value of the commutator in Eq. (3.2) can be rearranged using the cyclic property of the trace and the fact that one can regard the operator $\exp[-\beta\mathbf{K}_0]$ as generating displacements in imaginary time:

$\langle[\mathbf{j}, \rho_{\mathbf{G}}]\rangle = \langle \mathbf{j}(\rho(t) - \rho(t + i\hbar\beta))\rangle$. The difference of the density operators is then expressed as the integral of $\dot{\rho}$ over an auxiliary variable λ giving

$$\mathbf{J}(\mathbf{r}) = -e \lim_{\delta \to 0} \int_{-\infty}^{t} dt' e^{\delta t'} \cos \omega t' \int_{0}^{\beta} d\lambda \int d\mathbf{r}' \, \langle \mathbf{j}(\mathbf{r}, t - i\hbar\lambda) \, \dot{\rho}(\mathbf{r}', t') \rangle \, \phi(\mathbf{r}'), \tag{3.3}$$

where we have used the cyclic property of the trace to shift the argument of $\mathbf{j}$ by $-i\hbar\lambda$. We can now apply the continuity equation $e\dot{\rho}(\mathbf{r}, t') = -\nabla \cdot \mathbf{j}(\mathbf{r}, t')$ in the interaction picture to Eq. (3.3) and integrate by parts. This yields

$$\mathbf{J}(\mathbf{r}, \omega) = \lim_{\delta \to 0} \int_{-\infty}^{t} dt' e^{\delta |t'|} \cos \omega t' \int_{0}^{\beta} d\lambda \Big\langle \mathbf{j}(\mathbf{r}, t - i\hbar\lambda) \times \Big[- \int d\mathbf{r}' \mathbf{j}(\mathbf{r}', t') \cdot \nabla' \phi(\mathbf{r}') + \int_{s' \to \infty} ds' \, j_{\perp}(\mathbf{s}', t') \, \phi(\mathbf{s}') \Big] \Big\rangle, \tag{3.4}$$

where $j_{\perp}$ is the normal component of the current density, and the surface s′ must be taken to infinity because the original integral, Eq. (3.3), is of infinite range for the open system. In ref. [47] a careful argument is given demonstrating that the surface term vanishes as long as the correct order of limits is taken: $\lim_{\delta \to 0} \lim_{\mathbf{r} \to \infty}$. Note that the bulk term is proportional to the electric field as we desired and only extends over the finite sample region $\mathcal{A}$ where the field is non-zero. Since the remaining bulk term has the form $\mathbf{J}(r, \omega) = \int \mathrm{d}r \sigma(\omega, r, r') \cdot \mathbf{E}(r')$, we can now identify the non-local conductivity tensor $\sigma(\omega)$ as an expectation value of the relevant product of current operators. This term can be expressed in terms of complete sets of (many-body) eigenstates $|\alpha\rangle, |\beta\rangle$ with energies E_α, E_β and the integrals over t' and λ can then be done. Taking the limit $\omega \to 0$ (but ωt finite) we find a purely dissipative DC response ($\sim \cos \omega t$) with

$$\sigma(r, r') = -i\hbar \lim_{\delta \to 0} \sum_{\alpha, \beta} \frac{P_\beta - P_\alpha}{E_\beta - E_\alpha} \frac{\langle \beta | \, j(\mathbf{r}) | \alpha \rangle \, \langle \alpha | j(r') | \beta \rangle}{E_\beta - E_\alpha + i\hbar\delta} \tag{3.5}$$

where $P_\alpha = (\rho_{\mathbf{G}})_{\alpha\alpha}$ is the thermodynamic occupation probability of many-body state α. As discussed above, this operator relates the current density to the external and not the total electric field, but this is sufficient for the purpose of obtaining the conductance coefficients.

The non-local conductivity tensor $\sigma(r, r')$ is a sample-specific quantity which may be defined for each impurity configuration, sample and measuring geometry. In general one does not expect this function to depend only on the difference $r - r'$

and one expects a spatially-varying current density $\mathbf{J}(r)$. If one averages this function over impurity configurations in the bulk one obtains of course a function of $r - r'$ which is often taken to be short-ranged and of the form $\overline{\sigma}(r, r') = \sigma_0 \exp[|r - r'|/l]$; thus the conductivity is taken to be local on a scale larger than the elastic mean free path. However this is not correct; Kane, Serota and Lee showed [53] that there are non-local contributions to both the average and variance of the Kubo tensor on the scale of the inelastic mean free path (leading to the non-local effects discussed in section (1.2)).

It can be shown [40] that the sample-specific conductivity tensor of Eq. (3.5) satisfies the generalized Onsager relation $\sigma_{ij}(r, r', B) = \sigma_{ji}(r', r, -B)$. It follows that the spatially-averaged $\sigma_{ij} = \int dr dr' \sigma_{ij}(r, r', B)$ will satisfy the familiar Onsager relation (by interchange of the dummy integration variables). *but this spatially-averaged conductivity cannot be directly measured in mesoscopic samples.* Hence the relevant time-reversal symmetry is the reciprocity symmetry discussed in section (2.3).

3.3. Conductance coefficients in linear response

The currents I_m in Eq. (2.2) are obtained by integrating the current density obtained from Eqs. (3.4,3.5) through the cross-section of lead m. Once this is done, we must integrate again by parts with respect to r' in Eq. (3.4) to express the I_m in terms of the voltages on the leads V_m. The bulk term in this integration then involves $\int \mathrm{dS_m} \nabla' \cdot \sigma$ which can be shown to vanish from current conservation [40] (S_m is the cross-sectional surface of lead m); the remaining surface terms give a contribution from each lead proportional to the voltage on that lead:

$$g_{mn} = -\int dy_m \int dy'_n \hat{\mathbf{x}}_m \cdot \sigma(r_m, r'_n) \cdot \hat{\mathbf{x}}'_n, \tag{3.6}$$

where y_m, x_m denote the transverse and longitudinal coordinates in lead m.

We note that Eq. (3.6) involves a surface integral of exactly the same form as the one in Eq. (3.4) which we claimed vanishes, *except that here there is no limit taking the surface to infinity*. Obviously Eq. (3.6) must be non-vanishing for our linear response calculation to be sensible, which raises the question of whether our treatment of the earlier surface term was consistent. In fact Sols has recently claimed [50] that this treatment *is* inconsistent and that the continuity equation must be altered "at infinity" to eliminate this earlier surface term. However the surface term in Eq. (3.4) *required* that the limit of the surface going to infinity be taken before the adiabatic limit $\delta \to 0$, whereas in (3.6) the limit $\delta \to 0$ is taken and then (if desired) the limit of the surface tending to infinity may be taken. Following [47] we show explicitly below that these limits do not commute and that there is no inconsistency.

Equations (3.5),(3.6) for the g_{mn} are valid in the presence of arbitrary interactions, but are not so useful microscopically in the general case. Thus we specialize to the case of non-interacting quasi-particles. In the non-interacting limit, the statistical weights P_α can be replaced by Fermi functions $f(E_\alpha)$, and $|\alpha\rangle$ become single-particle states. Once this is done equation (3.5) is often divided into two terms by applying the Cauchy principal value identity to the energy denominator: $[E_\beta - E_\alpha + i\hbar\delta]^{-1} = -\pi i\hbar\delta(E_\beta - E_\alpha) + P\{[E_\beta - E_\alpha]^{-1}\}$. The delta function term is symmetric in magnetic field (without interchanging $r \rightarrow r'$) while the principal value term is anti-symmetric, hence it must vanish at $B = 0$ [40]. The delta function term only involves states within kT of the fermi surface, whereas the principal value term appears to depend on all states beneath the fermi surface (and it is sometimes stated that the Hall conductivity arising from this term is not a fermi-surface quantity). By deriving Eq. (2.2) below we will demonstrate that the Hall resistance is in fact completely expressible in terms of transmission coefficients at the fermi surface, a non-trivial result. To achieve this it turns out to be more convenient to work with the sum of the symmetric and anti-symmetric parts as in Eq. (3.5).

The relevant single-particle states for our model are scattering states which may be expressed in the leads in terms of the elements of the scattering matrix S; in lead l, they have the asymptotic form

$$\psi^l_\alpha \equiv \psi^l_{Eap} \equiv \delta_{pl}\,\xi^l_{-a} + \sum_{a'} S_{lp,a'a}\,\xi^l_{+a'}. \tag{3.7}$$

Here, the label α consists of the energy E, subband index a and lead p of the incident wave. An analogous definition holds for $\psi^l_\beta \equiv \psi^l_{E'bq}$. The quantum wire eigenfunctions have the form

$$\xi^l_{\pm a}(\mathbf{r}) = \left|2\pi\,\frac{dE^l_a}{dk}\right|^{-1/2} e^{i\mathrm{k}^l_{\pm a}x}\,\chi^l_{\pm a}(y), \tag{3.8}$$

where $\chi^l_{\pm a}$ are the transverse wavefunctions and $\mathrm{k}^l_{\pm a}$ is the outgoing (+) or incoming (−) wavenumber. With the above choice of normalization, the symbolic sums over collective labels have the explicit form $\sum_\alpha \rightarrow \sum_p \sum_a \int dE$. In the following, subscripts a imply a dependence on the energy variable E, while indices b belong to energies E'. As was shown in Ref. [40], current conservation implies the following properties for two wire eigenfunctions at the same energy in the asymptotic region:

$$\int dy_l\,(\xi^l_{\sigma a}|j_\perp(\mathbf{r})|\xi^l_{\sigma' a'}) = \sigma\frac{e}{2\pi\hbar}\,\delta_{\sigma'\sigma}\delta_{a'a}, \tag{3.9}$$

with the notation $\sigma = \pm$, and round brackets for the single particle current matrix elements. If ϵ^l_a is the propagation threshold of subband a in lead l, the summations

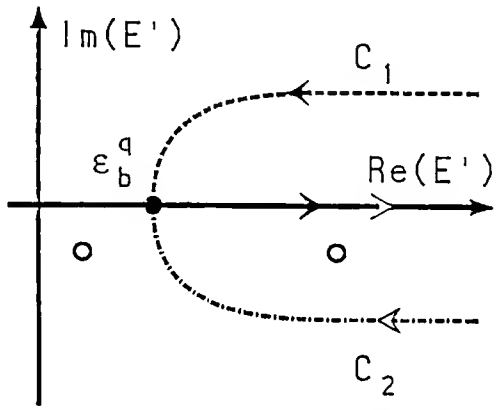

Fig. 6. The two possible contours that yield exponential decay in x' off the real axis for the various terms in Eq. (3.13). Open dots: two possible locations of the pole at $E' = E - i\hbar\delta$.

in Eq. (3.5) lead to integrals of the type

$$\int_{\epsilon_a^p}^{\infty} dE \int_{\epsilon_b^q}^{\infty} dE' \, \frac{f(E') - f(E)}{E' - E} \, \frac{F_S(E', E)}{E' - E + i\hbar\delta}, \tag{3.10}$$

where

$$F_S(E', E) \equiv \int_S ds' (\psi^m_{E'bq} | j_\perp(\mathrm{r}) | \psi^m_{Eap}) (\psi^n_{Eap} | j_\perp(\mathrm{s}') | \psi^n_{E'bq}) \tag{3.11}$$

contains the current matrix elements and thus vanishes at threshold. The surface S of integration is the surface of the *sample* region, $\partial\mathcal{A}$. Although we wish to let $\partial\mathcal{A} \to \infty$ eventually, we can do so only after $\delta \to 0$.

We now evaluate the integral over E' in Eq. (3.10) by Cauchy's theorem: a similar approach is taken in Refs. [51,52]. In general the integrand in Eq. (3.10) may have a complicated singularity structure in the complex plane, arising both from the "Matsubara" poles of the first factor and the singularities of the S-matrix contained in $F_S(E, E')$. However since asymptotically the wavefunctions have a plane-wave dependence on x' (the longitudinal coordinate in the lead), we shall see that contributions from the return contour may always be made to vanish as long as the correct half-plane is chosen to close the contour.

Since the locations of all the singularities of the integrand in Eq. (3.10) are independent of both the asymptotic and adiabatic limits except for the pole at $E' = E - i\hbar\delta$, for convenience we choose contours C_1, C_2 (shown schematically in Fig.) which by assumption enclose only the latter pole. Hence C_1 will contain no singularities at all, and terms which in the asymptotic limit may be closed in the upper-half plane will give zero contribution. C_2 will enclose the pole at $E' = E - i\hbar\delta$ unless it approaches the real axis outside the range of the E' integration (i.e. unless E is less than the sub-band threshold relevant for the term

in question). By this convenient choice of contours we need only evaluate the residue at $E' = E - i\hbar\delta$.

The residue theorem yields with $\nu = 1, 2$

$$\left(\int_{\epsilon_b^q}^{\infty} dE' + \int_{C_\nu} dE' \right) \frac{f(E') - f(E)}{E' - E} \frac{F_S(E', E)}{E' - E + i\hbar\delta} = -2\pi i \, \delta_{\nu,2} \, \Theta(E - \epsilon_b^q) \frac{f(E - i\hbar\delta) - f(E)}{-i\hbar\delta} F_S(E - i\hbar\delta, E), \tag{3.12}$$

where the step function Θ enters since C_2 encloses a pole only if $E > \epsilon_b^q$, and $\delta_{\nu,2}$ reflects the fact that no poles are enclosed by C_1. Along C_ν, the limit $S \to \infty$ enables us to apply the asymptotic forms of ψ_α and ψ_β in the second current matrix element in $F_S(E', E)$ to get in lead l

$$(\psi^l_{Eap}|j_\perp(\mathrm{s}')|\psi^l_{E'bq}) = \delta_{ql}\,\delta_{pl}\,(\xi^l_{-a}|j_\perp|\xi^l_{-b}) + \delta_{pl}\sum_{b'} S_{lq,b'b}(\xi^l_{-a}|j_\perp|\xi^l_{+b'}) + \delta_{ql}\sum_{a'} S^*_{lp,a'a}(\xi^l_{+a'}|j_\perp|\xi^l_{-b}) + \sum_{a'b'} S^*_{lp,a'a} S_{lq,b'b}(\xi^l_{+a'}|j_\perp|\xi^l_{+b'}), \tag{3.13}$$

irrespective of whether $\delta = 0$ or not in Eq. (3.12). For E' in the complex plane, the imaginary parts of the wavenumbers satisfy

$$\mathrm{sgn}\left(\mathrm{Im}\,\mathrm{k}^l_{\pm b}(E')\right) = \pm\mathrm{sgn}\left(\mathrm{Im}\,E'\right). \tag{3.14}$$

This can easily be checked for the special case $\mathrm{k}^l_{\pm b} \propto \pm\sqrt{E' - \epsilon_b^q}$, but holds even in asymmetric leads at $B \neq 0$ where $E' = \epsilon_b^q$ can occur for nonzero k. Note that the branch point at ϵ_b^q causes no problems since $F_S(E', E)$ vanishes there. The first and third term of Eq. (3.13) depend on $\xi^l_{-b} \propto e^{i\mathrm{k}^l_{-b}x'}$, so that they acquire an exponential decay factor $e^{-\kappa(E')x'}$ when integrated along the contour C_2. For the other two terms in Eq. (3.13), we choose C_1 to obtain positive imaginary parts in $\mathrm{k}^l_{+b}(E')$. The asymptotic limit $x' \to \infty$ causes the contributions from C_1 and C_2 to vanish identically. The result is that the real axis integrals over E' in Eq. (3.10) vanish due to Cauchy's theorem unless C_2 encloses a pole. Its residue in Eq. (3.12) contains a factor $e^{i\mathrm{k}^l_{-b}(E - i\hbar\delta)x'}$. For $E \neq \epsilon_b^q$ we can expand the outgoing wavenumber as $\mathrm{k}^l_{-b}(E) - i\delta\, v^{-1}(E)$ where the group velocity $v(E) = (1/\hbar)dE/dk$ is negative. We thus pick up a decaying exponential of the form

$$F_S(E - i\hbar\delta, E) \propto \exp\left[-\delta\,\left|v^{-1}(E)\right|\,x'\right]. \tag{3.15}$$

This exhibits clearly the noncommutativity of the limiting procedures: If we take $x' \to \infty$ first as we were *required* to do in the surface term of Eq. (3.4) then this

term vanishes. On the other hand, the g_{mn} of Eq. (3.6) are nonzero because there we are required to take $\delta \to 0$ first in Eq. (3.15), yielding

$$\lim_{\delta \to 0} \int_{\epsilon_b^q}^{\infty} dE' \, \frac{f(E') - f(E)}{E' - E} \, \frac{F_S(E', E)}{E' - E + i\hbar\delta} = -2\pi i \, \delta_{\nu,2} \, \Theta(E - \epsilon_b^q) \, f'(E) \, F_S(E, E). \tag{3.16}$$

This result leads to Eq. (2.2), as we now show by taking the asymptotic limit $S \to \infty$. The product of current matrix elements at the same energy in $F_S(E, E)$ can be evaluated with Eq. (3.13) if we let $\mathbf{r}$ go to infinity as well. Considering only $n \neq m$, 7 of the 16 terms in $F_S(E, E)$ vanish identically due to Kronecker delta factors like $\delta_{pm}\delta_{pn}$. When the sums over the incident wave parameters p, a or q, b are performed five more terms drop out due to the unitarity of the S matrix [47], two of the remaining four vanish due to integration along C_1 (see 3.16) and one vanishes due to Eq. (3.9).

Thus our expression for g_{mn} now contains only one term:

$$\begin{aligned} g_{mn} = i\hbar \int dy_m \int dy_n \sum_{p,q=1}^{N} \sum_{a,b=1}^{\infty} (-2\pi i) \int_{\epsilon_a^p}^{\infty} dE \, \Theta(E - \epsilon_b^q) \, f'(E) \\ \times \delta_{qn}\delta_{pn} \sum_{a'b'} \left[S^*_{mn,b'b} S_{mn,a'a} \left(\xi^m_{+b'} | j_\perp | \xi^m_{+a'} \right) \left(\xi^n_{-a} | j_\perp | \xi^n_{-b} \right) \right]_{E'=E} \\ = \frac{e^2}{h} \int_{\epsilon_1^n}^{\infty} dE \, \left[-f'(E) \right] \sum_{a'a}^{E} |S_{mn,a'a}|^2 , \end{aligned} \tag{3.17}$$

where Eq. (3.9) has been used. This is the desired result, Eq. (2.2). We note that the term identical to this one with the lead indices reversed vanished above due to the sign of δ (which required integration along C_1); i.e. due to the adiabatic switching on of the perturbation from $t = -\infty$. So the causality requirement that g_{mn} depend only on scattering probabilities from n to m, and not vice versa is correctly represented by this procedure

4. Ballistic transport phenomena

4.1. Novel phenomena in high-mobility microstructures

We have shown above using physical arguments and linear response theory that the transport properties of mesoscopic conductors can be plausibly related to a

quantum many-channel scattering problem. One of the first and most important applications of this scattering approach was to the Aharonov–Bohm effect [54,55] and the universal conductance fluctuations in disordered microstructures [8,9,13,19]. These mesoscopic interference phenomena in disordered systems are reviewed in the chapters by Altshuler [16] and Bouchiat [15]. For disordered systems the analytic technique of impurity-averaged perturbation theory is applicable and leads to powerful results (such as the universality of the conductance fluctuations). The scattering approach is primarily useful here for numerical simulations. On the other hand, starting roughly in 1987 [31,32,56,41,57,43,58–61], reduced dimension high-mobility GaAs microstructures became available for experimental study and a wide variety of novel transport phenomena were discovered. Since measurements could be made in such structures on a scale shorter than the bulk *elastic* mean free path, electronic motion was ballistic (at least over several collisions with the boundaries). In this case the scattering approach was found to be particularly useful since it allowed a simple modelling and in many cases a simple physical understanding of of the novel phenomena. We will review several examples in detail below.

In such microstructures the potential confining the electrons is approximately uniform in each straight segment of the structure so that the concepts of sub-bands and propagating channels apply within the structure itself (and not just in some idealized perfect leads). For this reason such segments are sometimes referred to as "quantum wires" or "electron waveguides". We have already discussed in section (2.4) the simplest consequence of such sub-band structure, the quantized two-probe point contact resistance [31,32]. Although multi-probe structures do not show resistance steps associated with sub-band threshholds, they do show sharp resistance minima at low temperature [61]. These fermi energy dependent features represent threshhold effects in the quantum S-matrix of the type already well-known in nuclear physics. Due to lack of space they will not be treated in any detail below.

The type of samples we shall consider in this section are GaAs microstructures with quasi-one-dimensional leads which either intersect to form a four-probe junction [56,58] (see Fig. (7)) or which enter and leave a larger 2D island (see insets to Figs. (10),(12)) of electrons [62,64,65]. In the case in which the island is strongly coupled to the leads it acts as a resonant cavity for the transmitted and reflected electrons; when it is isolated from the leads by a tunnel barrier it acts in some respects like an artificial atom, often referred to as a "quantum dot". We shall refer to the four-probe junctions and two-probe resonators as *quantum junctions*, reserving the term *quantum dot* for the tunneling systems. The quantum junctions are simpler in that straightforward use of the scattering approach for non-interacting electrons appears to describe many of their properties adequately. In the quantum dots the charging energy [62,63,66]

and Coulomb blockade [67] phenomenon determine the basic experimental observations. We shall not have space to treat the quantum dots in any detail, although we have argued that quantum interference of single electrons still plays a role [68].

The experimental transport phenomena discovered in the ballistic quantum junctions can be roughly divided into three categories: 1) *Classical Geometric Effects* which can be understood from classical scattering of ballistic electrons from the boundaries or geometric features of the junction. 2) *Quantum Threshhold Effects* which we will not discuss further. 3) *Quantum Interference Effects* which arise from interference of different electronic scattering trajectories. This interference gives rise to both conductance fluctuations (CF) and weak localization (WL) even though the conductor has negligible bulk disorder.

Although in the most general sense the ballistic WL and CF effects have the same physical origin as in disordered systems (which may be regarded as chaotic systems specified by a large number of parameters), these interference effects are interesting from the perspective of the theory of *quantum chaos* (quantum manifestations of chaotic classical dynamics) [69]. There are very few quantum systems which can be studied experimentally and which have simple enough dynamics that a detailed connection can be made between the classical and quantum properties via semiclassical quantum theory. Jalabert et al. [70] were the first to point out that ballistic quantum junctions might provide such a class of systems. In this case the statistical properties of the conductance were predicted to reflect the nature of the classical mechanics. If the system is fully chaotic certain statistical behavior has been predicted both for the WL and CF which will be discussed in detail below. But perhaps even more intriguing was the possibility of *determining* the nature of the classical dynamics from the analysis of the conductance statistics; i.e. distinguishing chaotic from regular dynamics. Since the underlying electron system has substantial electron–electron interactions. such experimental results would provide a strong confirmation of the quasi-particle picture of fermi liquid theory, in a regime in which it has never before been tested. In fact we shall see below that there is now fairly solid experimental support for the idea that mesoscopic conductance can distinguish classically chaotic from regular electron dynamics. In the next section we will develop the semiclassical formalism which can be used to understand both the classical and quantum-chaotic effects in these systems.

4.2. Semiclassical formalism

Our aim is to combine semiclassical quantum theory with the scattering approach of Eq. (2.2) to develop a semiclassical theory of ballistic junctions. Thus the

basic objects of interest are the conductance coefficients:

$$g_{mn} = \frac{e^2}{h} T_{mn} = \frac{e^2}{h} \sum_{a,b=1}^{N_c} T_{mn,ab}, \tag{4.1}$$

where a, b label the outgoing and incident channels in the leads. We will suppress the lead indices m, n henceforth and focus on the two-probe case (where the transmission coefficient directly yields the conductance) for simplicity. Assume a two-probe quantum juntion with the left lead joining the junction along the line $x = 0$ and the right lead joining along $x = L$(left inset, Fig. (12)). The transmission amplitude from a mode b on the left to a mode a on the right for electrons at the Fermi energy E is given by the projection of the retarded Green function (evaluated at the Fermi energy) over the transverse wavefunctions ϕ_b and ϕ_a of the incoming and outgoing modes [28]:

$$t_{ab} = -i\hbar (v_a v_b)^{1/2} \int dy' \int dy\, \phi_a^*(y')\, \phi_b(y)\, G(L, y'; 0, y; E). \tag{4.2}$$

Here the integrals over y, y' are over the transverse cross-sections of the left and right leads as in section (3.3); the reflection amplitude is of the same form except that integrals are over the same lead and there is an additional term δ_{ab} representing the incoming wave.

This equation is exact and is the basis for the numerical results given below in which the exact Green function is found using a recursive algorithm which is described in detail in ref. [71]. It also provides an appropriate starting point for the semiclassical approximation to the transmission and reflection amplitudes. We proceed by replacing the Green function G in Eq. (4.2) by its semiclassical path-integral expression [69]

$$G^{\rm scl}(y'; y; E) = \frac{2\pi}{(2\pi i\hbar)^{(3/2)}} \sum_{s(y,y')} \sqrt{D_s} \exp\left(\frac{i}{\hbar} S_s(y', y, E_F) - i\frac{\pi}{2}\mu_s \right), \tag{4.3}$$

given as a sum over *classical trajectories* s between points y and y' of the entrance and exit cross sections (hereafter we will not write any x dependence). Here θ and θ' are the incoming and outgoing angles, $D_s = (m/v|\cos\theta'|)\ |\ (\partial\theta/\partial y')_y\ |$, S_s is the action integral along the path, and μ is the Maslov [69] index given by the number of constant-energy conjugate points.

In the case of hard-wall leads, the transverse wavefunctions have the form: $\phi_b(y) = \sqrt{2/W}\ \sin(b\pi y/W)$. For large integers b the integral over y in Eq. (4.2) will be dominated by the stationary-phase contribution occurring for traject-

ories starting at points y_0 defined by

$$\left(\frac{\partial S}{\partial y}\right)_{y'} = -p_y = -\frac{\bar{b}\hbar\pi}{W}, \quad \bar{b} = \pm b, \tag{4.4}$$

that is, the dominant trajectories are those for which the initial transverse momentum equals the momentum of the transverse wavefunction. Performing also the y' integral by stationary-phase, we obtain

$$t_{ab} = -\frac{\sqrt{2\pi i\hbar}}{2W} \sum_{s(\bar{a},\bar{b})} \operatorname{sgn}(\bar{a}) \operatorname{sgn}(\bar{b}) \sqrt{\tilde{D}_s} \exp\left(\frac{i}{\hbar}\tilde{S}_s(\bar{a},\bar{b},E) - i\frac{\pi}{2}\tilde{\mu}_s\right), \tag{4.5}$$

where the sum is now taken over trajectories s between the entrance and exit cross sections with incoming and outgoing angles θ and θ' such that $\sin\theta = \bar{b}\pi/kW$ and $\sin\theta' = \bar{a}\pi/kW$. The reduced action is

$$\tilde{S}(\bar{a},\bar{b},E) = S(y_0', y_0, E_F) + \hbar\pi\bar{b}y_0/W - \hbar\pi\bar{a}y_0'/W, \tag{4.6}$$

the new pre-exponential factor is

$$\tilde{D}_s = \frac{1}{mv|\cos\theta'|}\left|\left(\frac{\partial y}{\partial\theta'}\right)_{\theta}\right|. \tag{4.7}$$

(The explicit form of the new Maslov index, $\tilde{\mu}$, is known [72] but will not be needed here.) In general there will exist families of trajectories which directly traverse the junction without scattering from the boundary for which the second stationary phase integration is invalid [72]; these direct trajectories lead to non-universal effects which we neglect in our discussion below. Experiments and simulations have typically employed geometries intended to minimize these effects.

Equations (4.1) and (4.5) express the conductance as a sum over certain pairs of classical paths. If we now specialize to junctions with a constant potential inside and hard wall boundaries ("billiards") the classical trajectories do not change with energy (or wavevector $k = \sqrt{2mE/\hbar}$) and it is convenient to express the semiclassical conductance as

$$T(k) = \sum_{a,b=1}^{N_c} T_{ab} = \frac{1}{2}\frac{\pi}{kW}\sum_{a,b}\sum_{s}\sum_{u} F_{a,b}^{s,u}(k), \tag{4.8}$$

$$F_{a,b}^{s,u}(k) = \sqrt{\tilde{A}_s\tilde{A}_u}\exp\left[ik(\tilde{L}_s - \tilde{L}_u) + i\pi\phi_{s,u}\right], \tag{4.9}$$

where s and u label the paths with entrance and exit angles $\sin\theta = b\pi/kW$

and $\sin\theta' = a\pi/kW$, the effective length is $\tilde{L}_s = \tilde{S}_s/k\hbar = S_s/k\hbar + y\sin\theta - y'\sin\theta'$, the Maslov indices are included in the phase-factor $\phi_{s,u}$(which we suppress henceforth), and $\tilde{A}_s = (\hbar k/W)\tilde{D}_s$. Note that by these definitions $\tilde{A}$ is independent of energy so that the only energy-dependence in the summands is the explicit k-dependence in the actions.

4.3. Classical two-probe conductance

The classical conductance may be obtained from the semiclassical formula (4.8) by approximating the mode summations by integrals over continuous angles θ, θ'. That this is correct may be seen by noting that the momentum $p = \hbar k$ is a classical quantity which must remain fixed in the classical limit ($\hbar \to 0$), thus requiring the limit $k \to \infty$ at the same time. Since the entrance angle $\sin\theta = b\pi/kW$, the allowed angles become continuous in the classical limit. Noting further that the number of channel $N_c = \mathrm{Int}\{kW/\pi\}$ we arrive at the prescription $(\pi/kW)\sum_b^{N_c} \to \int_{-1}^{1} \mathrm{d}\sin\theta$ and similarly for $\sin\theta'$ (the lower limit is -1 because the summation in Eq. (4.5) is over positive and negative a, b). With this substitution Eq. (4.8) becomes

$$T(k) = \frac{k}{2\pi}\int_{-1}^{1} d\sin\theta \int_{-\pi/2}^{\pi/2} d\theta' \sum_{s,u}\left|\left(\frac{\partial y_s}{\partial\theta'}\right)\left(\frac{\partial y_u}{\partial\theta'}\right)\right|^{1/2} \exp\left[\frac{i}{\hbar}(\tilde{S}_s - \tilde{S}_u)\right]. \tag{4.10}$$

Equation (4.11) indicates that some further thought is required to get a meaningful classical limit for the conductance. Obviously $\lim_{k\to\infty} T(k)$ is not well-defined since it diverges as k and apparently oscillates indefinitely due to the k-dependent phases in the summation. The divergence is real in the sense that the conductance of the ballistic microstructure really is proportional to $N_c = \mathrm{Int}\{\mathrm{kW}/\pi\}$. The useful classical quantity to describe the system is not the transmission coefficient (which is normalized to N_c), but the transmission *probability* normalized to unity for perfect transmission $\mathcal{T} = T/(kW/\pi)$. This quantity is finite as $k \to \infty$ but still will have the rapid phase oscillations for any finite k. These rapid oscillations (which are just the conductance fluctuations with energy) will turn out to be order unity in T implying that they are order $1/N_c$ in $\mathcal{T}$; hence they will tend to zero as $k \to \infty$. However a convenient and physical method of eliminating them at this point is to define the average of $\mathcal{T}$ over wavevector k. This method is physical because a non-zero temperature will have essentially the same effect and the classical ballistic effects of interest are observed precisely at intermediate temperatures for which the inelastic scattering length is of order the size of the microstructure but the temperature is high enough to aver-

age out the quantum interference effects. The average of a quantity $A(k)$ will be defined as:

$$\langle A \rangle \equiv \lim_{q \to \infty} (1/q) \int_{q_c}^{q_c+q} dk A(k), \quad q_c W/\pi \gg 1. \tag{4.11}$$

Note that in principle we begin averaging at $q_c \gg \pi/W$ so that the semiclassical approximation is valid over the entire range. If we divide Eq. (4.10) by kW/π and perform the k average then since k only appears in the exponents we obtain rigorously [72] zero contribution unless the paths s, u have the same actions. If we neglect for the moment paths with the same action due to an exact symmetry (to be discussed in the WL section below) then only terms with $s = u$ contribute to the sum. Noting that for the diagonal terms $s = u$ the integral over outgoing angle θ' can be combined with the factor $\partial y_s/\partial \theta'$ to yield an integral over the *initial* position y, the remaining integrals can be expressed in the form:

$$\mathcal{T} = \frac{1}{2} \int_{-1}^{1} d(\sin\theta) \int_0^W \frac{dy}{W} f(y, \theta), \tag{4.12}$$

where $f(y, \theta) = 1$ if the trajectory with initial conditions (y, θ) is transmitted and $f(y, \theta) = 0$ otherwise. $\mathcal{T}$ in Eq. (4.12) may be calculated by a completely classical simulation, i.e. by injecting an ensemble of point masses into the junction and counting the fraction transmitted for a given magnetic field and geometry. The "classical" approximation to the quantum conductance is just

$$g = \frac{e^2}{h} \frac{kW\mathcal{T}}{\pi}. \tag{4.13}$$

This equation generalizes to the multi-probe conductance matrix g_{mn} simply by the replacement $\mathcal{T} \to \mathcal{T}_{mn}$; it was first introduced to describe ballistic junctions by Beenakker and van Houten [73] using a different argument. Equation (4.13) may also be derived from a Boltzmann equation approach [71]. The notion that the classical transmission probability can be used in the two-probe or multi-probe conductance formulas is not particularly surprising. However the present argument allows one to determine the correct initial distribution of injected particles (uniform in space and with weight $\cos\theta$ in momentum) and more importantly provides a natural generalization to the WL and CF effects.

4.4. Classical effects in ballistic junctions

Perhaps the first novel transport phenomenon discovered experimentally in ballistic junctions was "quenching" of the low-field Hall resistance. Roukes et al. [56] and subsequently several other groups [57–59] observed that the low field Hall resistance of ballistic junctions was strongly suppressed up to some field at

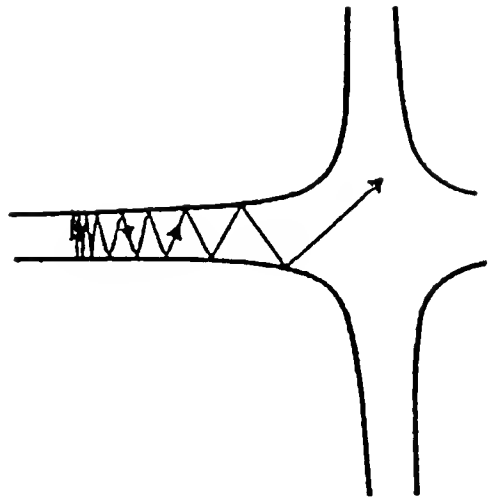

Fig. 7. Schematic showing collimation in the forward direction of a classical particle as it enters a rounded 4-probe junction.

which it rose sharply, overshooting the bulk 2D value and flattening out again to form a plateau (similar to quantum Hall plateaus but not at a quantized value of R_H). This effect as measured in the later experiment by Ford et al. [58] is shown in Fig. 4. Although initially a number of theoretical explanations for the effect were proposed, it is now fairly well accepted that it is due to geometric features of the junction and has an essentially classical origin (in the sense that Eq. (4.13) is classical). The particular property of the junction which was found to lead to quenching was the widening of the leads as the junction is approached (see Fig. 7). This widening is almost unavoidable experimentally because the conducting regions of the GaAs microstructure are defined by electrostatic gates placed in layers substantially above the two-dimensional electron gas. The spacer layer between the 2DEG and the gates is essential to get the high mobility, but it means that geometric features patterned in the gate are smoothed out at the level of the 2DEG. The widening of the leads creates a tendency for the entering electrons to have their momentum rotated from the transverse to the longitudinal direction (see Fig. 7), i.e. the electrons are *collimated* in the forward direction as they enter the junction. For this to occur the widening must be "adiabatic": the leads must widen gradually enough that the change in transverse momentum between collisions with the side wall is small compared to the initial transverse momentum [36,75,76]. Baranger and Stone [74] were the first to point out that this collimation could explain the quenching phenomenon.

If one assumes that the four-probe ballistic junction has four-fold rotational symmetry (as was approximately true in the experimental structures) the Hall resistance of Eq. (2.2) can be written in a simple form in terms of the transmission

coefficients T_R, T_L, T_F (transmission coefficients for the right,left and forward lead):

$$R_H = \frac{h}{e^2} \frac{(T_R + T_L)(T_R - T_L)}{D(T_R, T_L, T_F)}. \tag{4.14}$$

Here the denominator $D(T_R, T_L, T_F)$ is a sub-determinant of the conductance matrix [74]; it is relatively insensitive to magnetic field and its explicit form will not be needed. Note that R_H is proportional to the asymmetry $T_R - T_L$ in left-right transmission induced by the field, as one might expect. However R_H is also proportional to the *total sideways transmission* $T_R + T_L$; Baranger and Stone argued that this factor is suppressed by the collimation effect induced by the widening of the leads. They were able to establish [74] by quantum simulations of equation (4.14) that widened leads were essential to obtain generic quenching (for example a perfect square cross junction did not show quenching after averaging over energies (see Fig. 8)). The simulations at $T = 0$ also showed the large quantum conductance fluctuations which will be the subject of section (4.9) and it was only after including the effects of temperature by energy-averaging that generically flat low field Hall resistance was found (again see Fig. 8).

The simulations also clearly indicated that quenching did not arise solely from the suppression of sideways transmission [74]; it was found numerically that the widening of the leads was also reducing the asymmetry factor in R_H, $T_R - T_L$. At roughly the same time and independently, Ford et al. [58] proposed a simple mechanism for the asymmetry reduction. If the junction widens gradually electrons diverted by the field towards the left probe might rebound into the opposite ("wrong") probe (see inset to Fig. 4). The experimental data of Fig. 4, which were obtained from junctions intentionally fabricated to enhance this effect, dramatically confirm it. At an intermediate field the sign of the asymmetry is actually reversed, leading to an *inverted* Hall resistance (i.e. voltage induced opposite to the Lorentz force). This and other related experiments [58,59] established that junction geometry was crucial.

Shortly thereafter Beenakker and van Houten [73] proposed that the quenching, inversion and last plateau observed in the Hall resistance of ballistic junctions could all be explained in terms of Eq. (4.13) as classical magneto-size effects. By classical simulations of the type described after Eq. (4.12) they were able to reproduce the experimental results qualitatively and semiquantitatively. They went on to suggest that yet a third mechanism might be important in the quenching which they referred to as "scrambling". The idea was that the rounded junction allowed long trapped trajectories which would "forget" which lead they had entered from and hence which Hall probe the field was favoring. Subsequently Baranger et al. [71] performed detailed classical and quantum simulations of four-probe junctions looking at both the Hall and longitudinal resistance (which is often re-

ferred to as the "bend" resistance since the current turns a corner). They looked carefully at the three classical mechanisms for quenching: 1) Forward transmission enhancement. 2) Rebound mechanism. 3) Scrambling. It was shown from classical simulations that the asymmetry $T_R - T_L$ was determined almost completely by short trajectories and that while the rebound and forward enhancement effects were both important for the quenching, the scrambling mechanism was not significant [77]. The classical model for the last plateau and bend resistance also achieved reasonable success. In summary, the classical conductance formulas Eqs. (4.12), (4.13) provide a simple and reasonably good description of the magnetotransport through ballistic junctions, *in the temperature range* $1 - 4K$.

4.5. Quantum ballistic effects

The classical theory works well at intermediate temperatures but begins to fail badly as the temperature is lowered another order of magnitude. One source of the failure is the quantum threshhold effects [61] mentioned above which become more pronounced as temperature smearing is reduced. However the more interesting source of failure is the appearance of interference effects associated with multiple bounce trajectories trapped in the junction. In Fig. 8 (top) we show the Hall resistance of a ballistic junction at 100mK; although one can make out a tendency towards quenching, superimposed on this smooth classical magneto-size effect are reproducible fluctuations similar to the UCF of disordered microstructures. The presence of the quenched envelope in the data is important because it indicates that the transport is truly ballistic and hence the fluctuations are not simply due to disorder arising from poor sample fabrication. In Fig. 8 (bottom) we show theoretical calculations which compare the classical and quantum predictions for the the Hall resistance of ballistic junctions. As suggested by the experiment of Fig. 8, the classical simulation reproduces the quenching behavior but not the fluctuations, which in the quantum simulations occur both as a function of magnetic field and energy. Simulations demonstrate that a rounded four-probe junction definitely generates chaotic scattering for the trajectories which remain in the junction for many bounces [70,78]. But the classical transport coefficients of Eq. (4.12) involve a phase-space average over many trajectories which smooths out the strong dependence on external parameters of the individual chaotic trajectories. *Classical* chaos is not easily observed in ballistic microstructures. Although the fluctuations were observed experimentally as early as 1988 [57], it wasn't until after their connection with quantum chaos was proposed in 1990 [70] that they became the object of intensive study [64,65,79–83]. However the occurence of the fluctuations is not a unique signature of quantum chaos. Both chaotic and integrable cavities exhibit such fluctuations [72]; it is only their statistical properties which differ in the two cases (as we shall see in detail below).

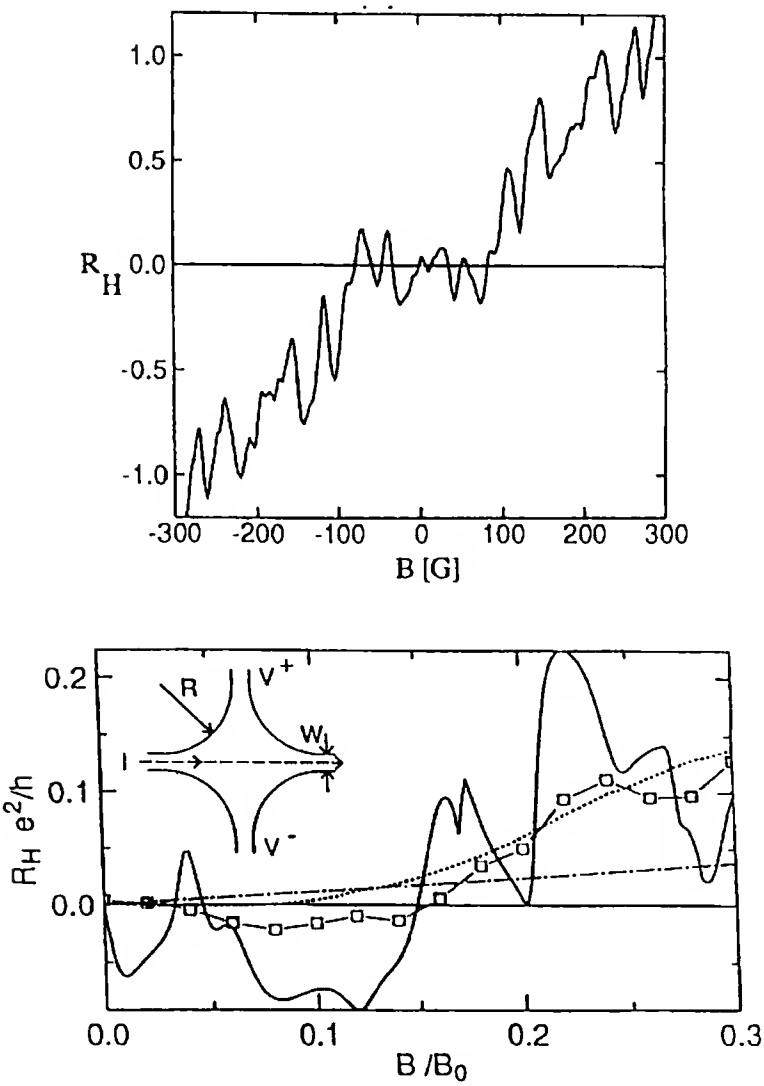

Fig. 8. (Top) Experimental Hall resistance from ballistic junction at 100 mK (adapted from [60]). (Bottom) Four calculations of the $T = 0$ Hall resistance of a ballistic junction: (dashed) Classical calculation from Eq. (4.12) showing quench but no fluctuations. (dash-dot) Quantum square-corner junction ($R/W = 0$) from Eq. (4.1) showing no fluctuations due to lack of trapped trajectories. (Solid line) Quantum rounded junction showing fluctuations. (Squares) Energy-averaged quantum calculations for the rounded junctions showing quenching. Inset: Schematic of rounded junction, results are for $R/W = 4$. R_H is in units h/e^2, B in units $B_0 = mcv_f/eW$.

Keller et al. [65] were the first to fabricate microstructures of the relevant type in which the electron density (and hence the fermi momentum k_f) was tunable while maintaining the geometry approximately fixed. Some representative data from their measurements is shown in Fig. 9. Here ballistic conductance fluctuations are plotted vs. k_f for several values of the magnetic field. One sees that on average increasing the B field increases the conductance: this is the ballistic weak localization effect. It is more difficult to observe in ballistic microstructures because the averaging out of the fluctuations must be done explicitly (either

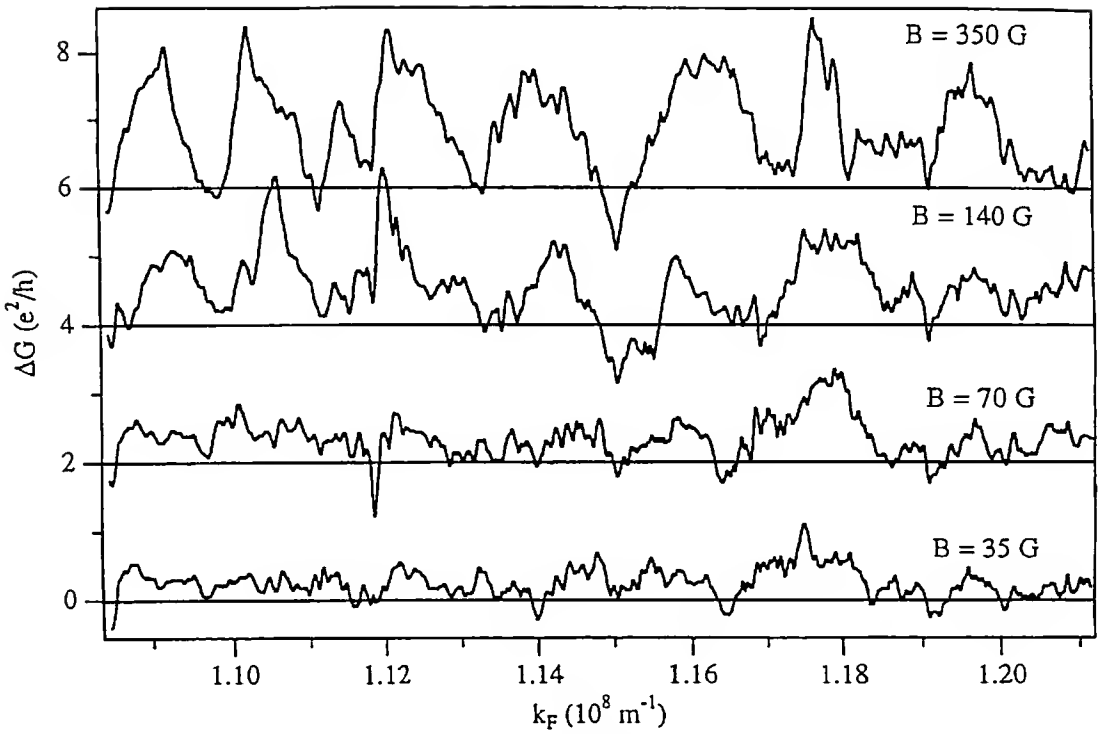

Fig. 9. Measured conductance fluctuations as a function of k_f in a ballistic junction at magnetic fields varying from 35 to 350 G. ΔG denotes the difference $G(B, k_f) - G(0, k_f)$ and is typically positive due to WL effect (Adapted from [83]).

by varying the fermi energy [65] or by making many similar samples in parallel [81]), in contrast to disordered systems where studying samples much longer than the phase coherence length leads to self-averaging of the fluctuations. Figs. 8, 9 shows that both the WL and CF effects exist in the ballistic regime. As in disordered microstructures the origin of the effects is constructive interference of time-reversed pairs of electron trajectories in the case of WL [4,16,84] and interference of more general trajectories with a field and energy-dependent phase for the case of CF [8]. However in the ballistic case a more detailed semiclassical theory is possible. Also it is now understood that there are subtle statistical differences between the disordered and ballistic effects (see section 4.11 below).

4.6. Ballistic weak localization: coherent backscattering

Although the conductance fluctuations are the most prominent feature of the data in Figs. (8),(9), the weak localization effect is a simpler starting point for the semiclassical theory and demonstrates both its strengths and weaknesses. In the discussion of the classical conductance in section (4.3) the interference of unlike paths in Eq. (4.10) was eliminated by the wavevector average (Eq. (4.11)) which introduced a delta function setting the effective actions $\tilde{S}_s = \tilde{S}_u$. At that point we neglected the possibility that unlike paths may have the same effective actions.

This may occur due to exact spatial symmetries of the confining geometry (we have discussed this case elsewhere [71]) but more importantly it will occur due to time-reversal symmetry. The breaking of this symmetry by a weak magnetic field leads to the WL effect in conductance which we now attempt to evaluate using the semiclassical theory.

In doing so we immediately encounter a conceptual difficulty. The semiclassical transmission amplitude t_{ab} of Eq. (4.5) is given by a sum over classical paths entering at the quantized angle $\sin\theta_b = \pm b\pi/W$ and exiting at $\sin\theta'_a = \pm a\pi/W$; the time-reverse of such a path *exits* at $\sin\theta'_b$ and *enters* at $\sin\theta_a$. Hence the time-reversed path contributes to t_{ba} and *does not interfere with the original path in the summation of Eq. (4.8)* (which is over $|t_{ab}|^2$). The only S-matrix elements in which exact time-reversed pairs interfere semiclassically are the diagonal elements of the reflection matrix, $R_{aa} = |r_{aa}|^2$. Hence it is only the effect of TR symmetry on $R_D = \sum_a^{N_c} R_{aa}$ that we can evaluate using the method of section (4.3). Obviously R_D is related to the transmission and off-diagonal reflection ($R_{OD} = \sum_{a\neq b}^{N_c} R_{ab}$) by unitarity: $R_D + R_{OD} + T = N_c$. Thus the failure of our semiclassical approach to find a direct WL effect in transmission is troubling; we shall return to this point below.

We first note that the semiclassical reflection amplitudes have exactly the same form as Eq. (4.5) except that both θ and θ' refer to the same lead and there is a term δ_{ab} representing the incoming wave. Since below we will be concerned only with the field-dependent correction to R_D we can neglect the δ_{ab} term. The relevant part of $R_D(k)$ in semiclassical approximation is:

$$R_D = \sum_a^{N_c} R_{aa} = \frac{1}{2}\frac{\pi}{kW}\sum_a\sum_{s,u} F_{a,a}^{s,u}(k), \tag{4.15}$$

where $F_{a,a}^{s,u}(k)$ is given by Eq. (4.9) generalized for reflection. R_D has a contribution from like paths $s = u$ of the type leading to Eq. (4.12); however this contribution is not sensitive to weak fields. Hence we immediately focus on the terms $s = T(u)$ in Eq. (4.15)(where T is the time-reversal operator). These terms will survive the wavevector average and give an order unity contribution to $\langle R(k)\rangle$ which we denote by $\delta R_D(B)$. At B=0 $\tilde{S}_{T(u)} = \tilde{S}_u$, $\tilde{D}_{T(u)} = \tilde{D}_u$ and since $|\sin\theta| = |\sin\theta'|$ for paths contributing to R_{aa} we can again use the relation $(\pi/kW)\sum_a^{N_c} \to \int_{-1}^{1} \mathrm{d}\sin\theta$ to obtain

$$\delta R_D(B=0) = \frac{1}{2}\int_{-1}^{1} d(\sin\theta) \sum_{s(\theta,\pm\theta)} \tilde{A}_s \equiv \frac{1}{2}\int_{-1}^{1} d(\sin\theta)\tilde{A}(\theta,\theta). \tag{4.16}$$

The quantity $\tilde{A}(\theta,\theta) = \sum_{s(\theta,\pm\theta)}(|W\cos\theta|)^{-1}|\partial y_s/\partial\theta|$ measures the stability

of classical paths which enter and exit at θ with respect to variations in the initial position. Note that in the calculation for $\mathcal{T}$ (the terms $s = u$ in Eq. (4.10)) the same quantity appears generalized to unequal θ, θ', $\tilde{A}(\theta, \theta')$. For chaotic classical scattering there is no reason to expect $\tilde{A}(\theta, \theta')$ to depend strongly on its arguments. Hence we make a *uniformity hypothesis*: $\tilde{A}(\theta, \theta) \approx \int_{-1}^{1} d(\sin\theta')\tilde{A}(\theta, \theta')$. Classical simulations indicate that this assumption is reasonably well satisfied in chaotic cavities without direct trajectories [72]. If we substitute the uniformity relation into Eq. (4.16) it becomes identical to $\mathcal{R}$, the classical reflection probability (defined in obvious analogy to $\mathcal{T}$ of Eq. (4.12)). Since the terms $s = u$ in the semiclassical sum will give exactly the same contribution to R_D at $B = 0$ this implies

$$R_D(B = 0) \approx 2\mathcal{R}. \tag{4.17}$$

Since off-diagonal reflection coefficients and transmission coefficients will not have the contribution from time-reversed pairs semiclassically we conclude that the diagonal reflection coefficients are on average twice as large as these other elements in the S-matrix. This factor of two enhancement of the backscattering due to phase coherence and time-reversal symmetry (also known as the elastic enhancement factor in nuclear physics) is well-known in the literature on weak localization [4].

4.7. Ballistic weak localization: field dependence

We now evaluate the effect of a magnetic field on the enhanced diagonal reflection. Introducing a magnetic field in general changes *both* the classical paths traversed and the action along a given path; however, we will be considering low-field effects in which the change in the geometry of the paths is negligible and only the phase difference which now appears between time-reversed paths is important. For time-reversed pairs this phase difference (which is essentially due to the Aharonov–Bohm effect) arises due to the different sign of the "enclosed flux", $(S_s - S_u)/\hbar = 2\Theta_s B/\phi_0$ where $\Theta_s \equiv (2\pi/B)\int_s \boldsymbol{A}\cdot d\boldsymbol{l}$ is the effective "area" enclosed by the path and $\phi_0 = hc/e$. Although we refer to Θ_s as an area, the paths we are considering are not in general closed loops and thus Θ_s is not itself a gauge-invariant quantity. We have checked that the statistical properties of Θ_s are gauge-invariant in the chaotic case. Neglecting the change in classical paths we find instead of Eq. (4.16)

$$\delta R_D(B) = \frac{1}{2}\int_{-1}^{1} d(\sin\theta) \sum_{s(\theta,\pm\theta)} \tilde{A}_s e^{i2\Theta_s B/\phi_0}. \tag{4.18}$$

We now wish to convert the sum over classical paths s to an integral over the effective area of the paths Θ. Note that in the summation a classical quantity $\tilde{A}_s$

is multiplied by a phase factor with a quantum scale $\phi_0 = hc/e$ so as $\hbar \to 0$ $\tilde{A}_s$ may be treated as slowly-varying with respect to the phase factor when we convert from a sum to an integral. Hence we obtain

$$\delta R_D(B) = \mathcal{R} \int_{-\infty}^{\infty} d\Theta P(\Theta) \exp[i2\Theta B/\phi_0], \tag{4.19}$$

where $P(\Theta)$ is the probability that a traversing classical path encloses an effective area Θ.

Both numerical calculations [70] and analytic arguments [85,86] have found that the area distribution for long orbits takes on a universal form for simple chaotic billiards: $P(\Theta) \propto \exp(-\alpha_{cl}|\Theta|)$, where the only parameter characterizing the classical phase space is the quantity α_{cl}, the inverse of the typical area enclosed by a scattering trajectory. The origin of this universal form may be understood qualitatively by the following argument [85,86,72]. First, the number of orbits which remain in the scattering region long enough to cover a distance L decays exponentially with L. Crudely the reason is that for long chaotic orbits the probability of escaping at each encounter with the boundary is a constant $p \ll 1$ given approximately by the ratio of the size of the opening to the perimeter of the billiard and is uncorrelated with previous bounces. Hence after n bounces $P(n) \sim e^{-n \ln p}$, and if d is the mean length traversed between bounces, $P(L) \sim e^{-(L/d)\ln p} = e^{-\gamma_{cl} L}$. Second, the area Θ_s of a given trajectory is essentially given by its winding number around a central point in the billiard times a typical area per circulation A_0 (it is precisely this if the field is replaced by an Aharonov–Bohm flux, as considered by Berry and Robnik [87]). For a chaotic system the area accumulates diffusively, as both senses of circulation occur with roughly equal probability for long orbits. Hence the mean winding number for an orbit of n bounces is zero and its variance $w_n^2 \sim n$ [87,85,86]. The distribution of areas for orbits of length L is then Gaussian with the variance $A^2 \approx (L/d)A_0^2$. Finally, in order to obtain the distribution of areas for orbits of all lengths one must integrate this against the exponential distribution of lengths discussed above. The leading behavior of this integral may be obtained by the method of steepest descent [85]: one finds the exponential form for $P(|\Theta|)$ with $\alpha_{cl} \sim \sqrt{\gamma_{cl} d}/A_0$ [89]. Numerical results shown in Fig. 10 clearly confirm this result for strongly chaotic scattering.

Assuming fully chaotic scattering we insert the exponential form into Eq. (4.19) and obtain a Lorentzian B-dependence,

$$\delta R_D(B) = \frac{\mathcal{R}}{1 + (2B/\alpha_{cl}\phi_0)^2}, \tag{4.20}$$

where the magnetic field scale is set by the flux through the typical area α_{cl}^{-1} in units of the $hc/2e$ (note the now-familiar appearance of the superconducting

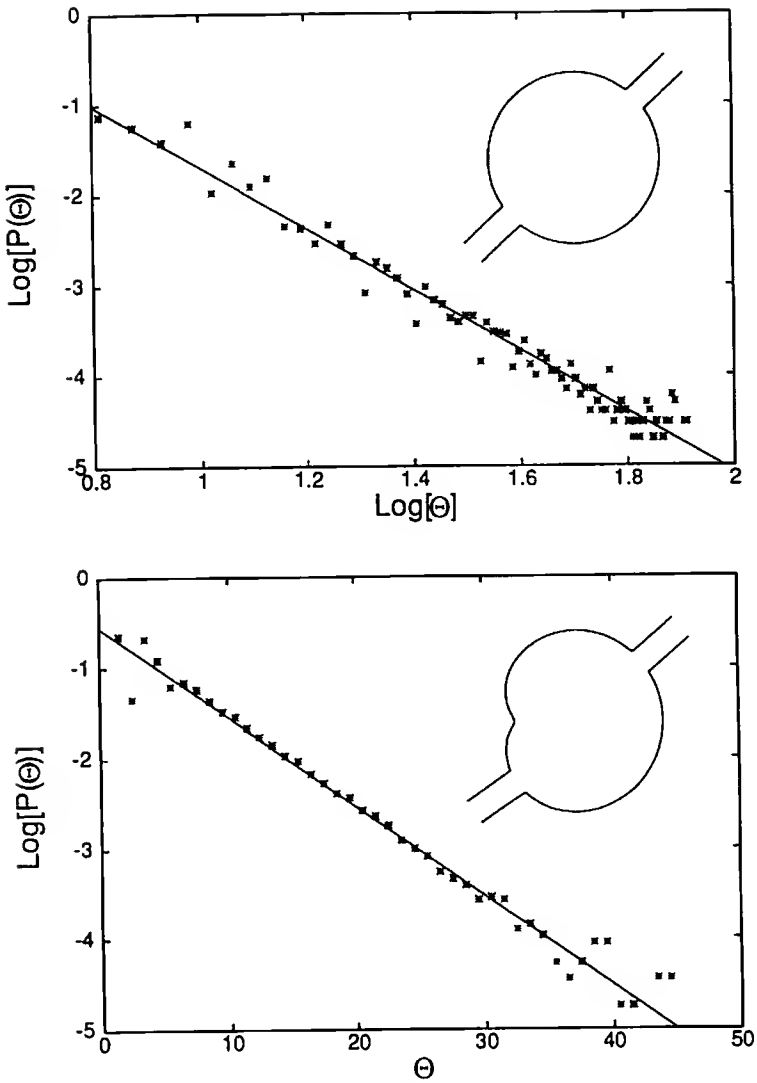

Fig. 10. Distribution of classical effective areas in scattering from circle (top) showing power-law shape and strongly-deformed circle (bottom) showing exponential form characteristic of chaotic scattering.

flux quantum in weak localization). So, as in the disordered case, for ballistic conductors with chaotic scattering, a weak magnetic field is sufficient to eliminate the enhanced backscattering. The effect this has on the conductance will be discussed in the next section.

4.8. Problems with unitarity

We have just shown using semiclassical theory that by application of a magnetic field $B \gg \alpha_{cl}\phi_0/2$ the diagonal reflection coefficient is reduced from $2\mathcal{R}$ to $\mathcal{R}$. By unitarity this means that $R_{OD} + T$ must increase by $\mathcal{R}$. However both R_{OD} and the conductance (in units e^2/h) T are of order N_c and in order to calculate $\delta T(B)$ we would need to evaluate them to order unity. But in section (4.3) we

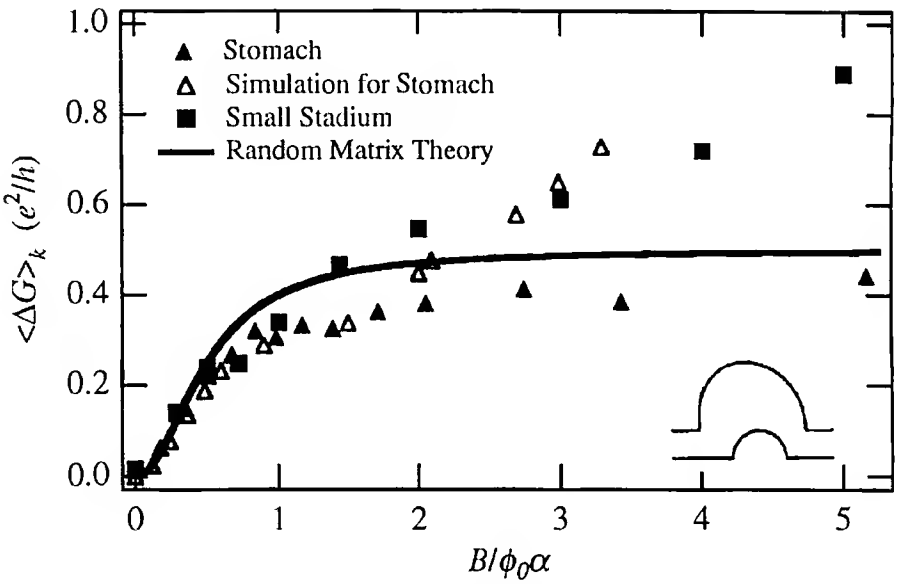

Fig. 11. Energy-averaged weak localization magnetoconductance from the experiments of Keller et al. obtained from data of the type shown in Fig. 9 compared to the prediction of Eq. (4.21) and of RMT. The parameter α used to scale the field axis was obtained from the conductance fluctuation power spectrum as discussed below, so there are no free parameters in the comparison. Inset shows one of the structures (referred to as the "stomach"). Also shown are numerical results from quantum simulations of the stomach. Adapted from [83].

were only able to evaluate T to order N_c ($\mathcal{T}$ to order unity), so we are unable to give a semiclassical prediction for $\delta T(B)$ itself. We can make the following hand-waving argument: for an ideal chaotic system where there are no short trajectories all memory of the incident lead would be "lost" on average and all exit channels would be equally probable. Thus $\mathcal{R} = \mathcal{T} = 1/2$ and since $R_{OD} \approx R$ to order N_c^{-1}, $\delta T = \delta R_{OD} = 1/4$, so that

$$\delta g(B) = \frac{e^2/2h}{1 + (2B/\alpha_{cl}\phi_0)^2}, \tag{4.21}$$

where we have now included for comparison with experiment the factor of two for spin. In fact exactly this result is obtained from a treatment using random-matrix theory [90]. However it must be admitted that a natural generalization of this argument to the disordered case gives gives a vanishing weak localization effect in quasi-1D [91], which is obviously incorrect.

In Fig. 11 equation (4.21) is compared with experiment and excellent agreement is found. We remind you that there simply were no exact time-reversed pairs interfering in the semiclassical sum for T (and R_{OD}) so this apparent failure of the semiclassical method points to a deeper problem with the method in this context which is not yet resolved [72]. Clearly one aspect of this difficulty is that T and R_{OD} must be evaluated to higher accuracy in the effective semiclassical parameter N_c^{-1} than R_D.

4.9. Ballistic conductance fluctuations

We will not present here the full semiclassical theory used to describe the ballistic conductance fluctuations; it is described in detail in [72]. The basic technique is the same as the approach used above to treat WL. Here the objects of interest are the correlation functions of the conductance as a function of wavevector and magnetic field

$$C(\Delta k) \equiv \langle \delta T(k + \Delta k)\delta T(k)\rangle_k \tag{4.22}$$

$$C(\Delta B) \equiv \langle \delta T(k, B + \Delta B)\delta T(k, B)\rangle_k, \tag{4.23}$$

where δT is defined by the deviation from the average value of section (4.3) in the absence of any symmetries, $\delta T \equiv T - TkW/\pi$. The calculation of both correlation functions follows closely the work by Blumel and Smilansky [92] who computed semiclassically the correlation functions (in energy) of the S-matrix elements of chaotic systems. The correlation functions involve a sum over four set of classical paths s, u, s', u' but with the terms $s = u, s' = u'$ subtracted out since (as we have seen) they contribute to the average transmission. Wavevector averaging then picks out only the terms $s = u', u = s'$ which are only present in $\langle \delta T_{ab}\delta T_{ab}\rangle$ (and not in terms of the form $\langle \delta T_{ab}\delta T_{cd}\rangle$). In the resulting sum all phase factors are canceled except for those arising from the difference $\Delta k, \Delta B$. It is natural then to compute the Fourier transform of these summations with respect to $\Delta k, \Delta B$ which we denote by $\widehat{C}(L), \widehat{C}(S)$ respectively; these are just the power spectra of the fluctuations. Straightforward manipulations show [72] that they can be expressed in terms of the convolution of the distribution of path lengths with itself (in the case of $\widehat{C}(L)$) and of effective areas $P(\Theta)$ with itself (in the case of $\widehat{C}(S)$). For the case of the length distribution (which is a simple exponential) its convolution is exponential with the same exponent, so $\widehat{C}(L) \propto \exp[-\gamma_{cl}L]$. The area distribution is exponential in the absolute value of Θ and so its self-convolution yields [70,72]:

$$\widehat{C}(S) \propto e^{-\alpha_{cl}|S|}(1 + \alpha_{cl}|S|). \tag{4.24}$$

Note again, as in WL, a parameter α_{cl} characterizing the average *classical* scattering dynamics determines a quantum property, in this case the power spectrum of the magnetoconductance fluctuations. A precise test of this semiclassical prediction is the following. First, an exact numerical solution for $T(B)$ for a given chaotic cavity is obtained. The power spectrum of the magnetoconductance fluctuations is fit to the semiclassical form (4.25) and the parameter α is extracted. Then $P(\Theta)$ is computed by Monte Carlo simulation of classical scattering in the same shape cavity and the parameter α_{cl} is extracted. According to the semiclassical theory these two parameters should agree when $N_c \gg 1$.

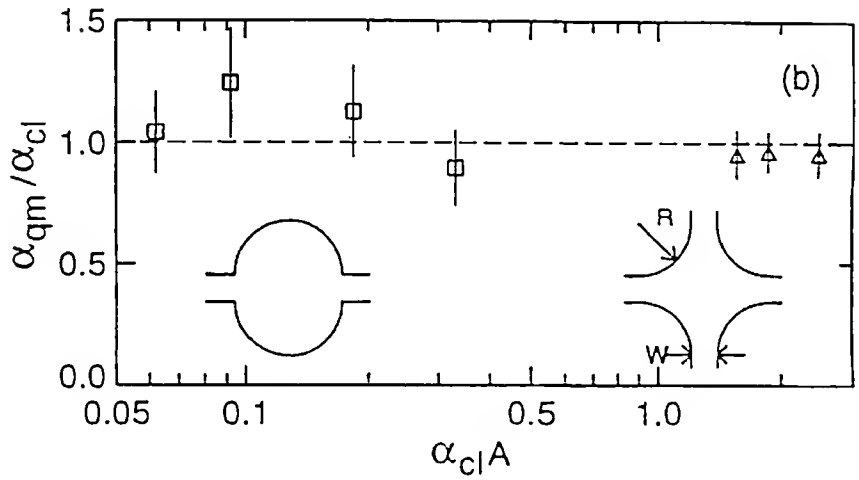

Fig. 12. Ratio of α obtained from quantum power spectra to that obtained from classical area distribution (see Fig. 10) for a range structures (see insets) vs. $\alpha_{cl}A$ where A is the area of the structure.

One finds [70,72] very good agreement over two orders of magnitude variation in α_{cl} (see Fig. 12). Several experiments [64,65] have analyzed their magnetotransport data in exactly this manner and found fair but not impressive agreement with theory (in the experimental case the potential defining the cavity is imperfectly known, and disorder [88] is apparently playing some role [89]).

4.10. Distinguishing regular from chaotic scattering

If the scattering is not chaotic (if e.g. the cavity is circular or polygonal) then the distribution of effective areas $P(\Theta)$ is not exponential, but typically is a power law as shown in Fig. 10 [72,89] (because there are many different time scales for escape in an integrable system, depending on the invariant torus in the neighborhood of the scattering trajectory). In this case one still expects WL and CF but with statistical properties different from those derived above assuming hard chaos. For example the dependence of the WL magnetoconductance on magnetic field should deviate from the Lorentzian of Eq. (4.21) and the power spectrum of the fluctuations should deviate from Eq. (4.24). The observability of these deviations is perhaps the most interesting aspect of this theory because it implies that through purely *quantum* measurements one can determine the nature of the *classical dynamics* of a quantum system. Although the arguments leading to Eq. (4.21) must be modified for integrable systems, we can estimate the WL lineshape in such systems by simply taking $P(\Theta) \sim \Theta^{-\beta}$ in Eq. (4.19) ($\beta \approx 3.3$ for the circle). Since Eq. (4.19) is (up to scale factors) just the Fourier transform of $P(\Theta)$ with respect to B one expects a cusp-like singularity in $\delta T(B)$ as $B \to 0$, since the Fourier transform of a pure power law must have a singularity in the some derivative as the transform variable tends to zero.

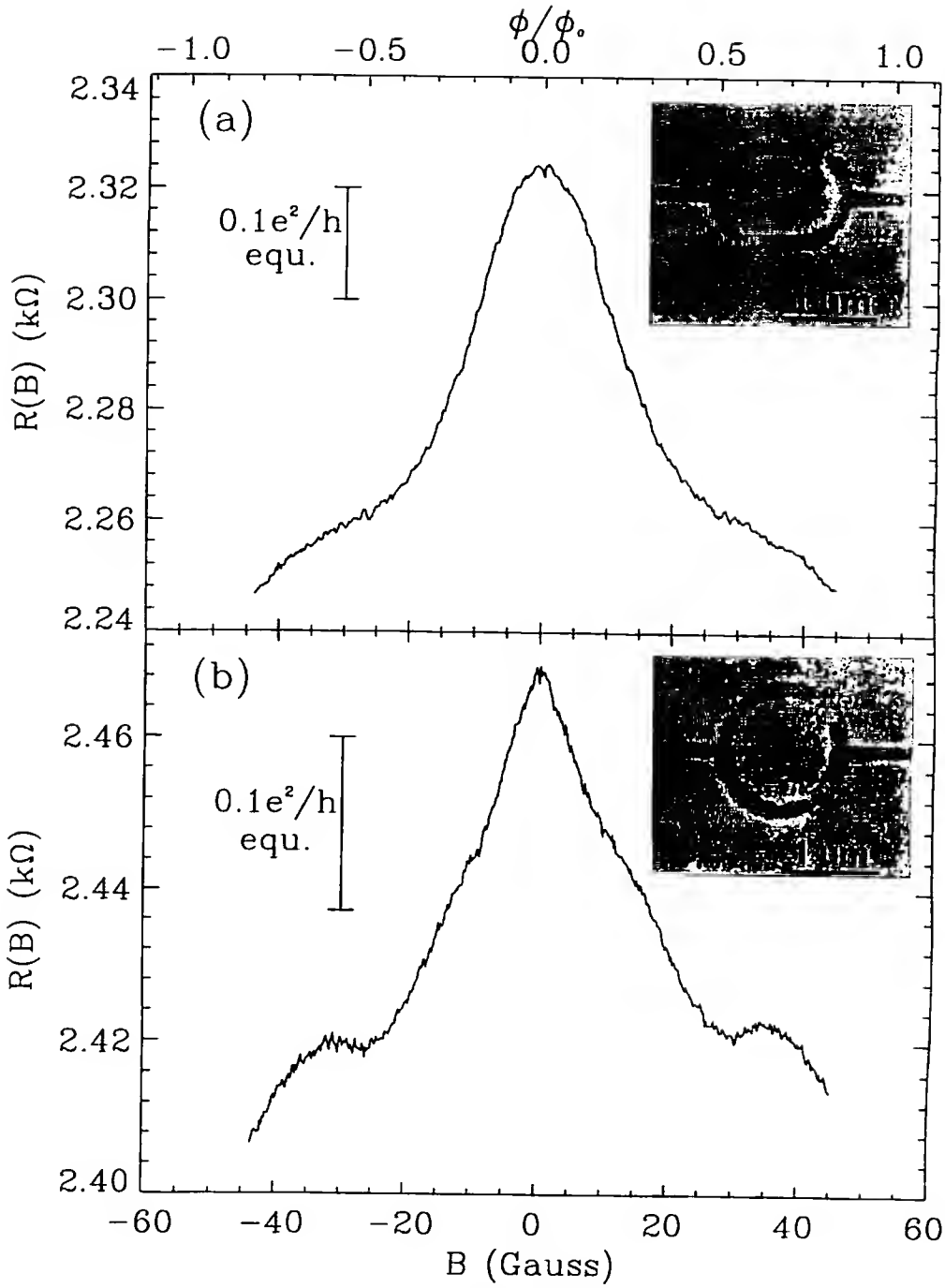

Fig. 13. Weak localization magnetoresistance for (a) 48 stadium cavities, and (b) 48 circle cavities measured at $T = 50$ mK. The circular (integrable) cavities show the remarkable cusp-like shape suggested by the semiclassical theory, whereas the stadium (chaotic) cavities do not. Reprinted from [81].

In Fig. 13 is shown WL magnetoresistance data from an experiment by Chang et al. [81] on ensembles of ballistic microstructures (measured essentially in parallel to average out the fluctuations). The ensembles differ only in the shapes of the electron cavities: stadium-like (top) and circular (bottom). Note the striking difference in the lineshape, the chaotic (stadium) ensemble showing smooth be-

havior as $B \to 0$ as compared to the regular(circular) ensemble showing a sharper cusp-like behavior as expected from our rough argument.

Well before this WL experiment Marcus et al. [64,79], motivated by similar reasoning, had studied the power spectra of magnetoconductance fluctuations in stadium and circular cavities. Since trapped trajectories in a circular cavity do not diffuse but instead circulate in a single sense one expects more enclosed flux on average and hence more high-frequency power over the same field range in comparison to the stadium structure. This effect was observed and although it is not as dramatic in the data as the effect shown in Fig. 13, together these two experiments provide solid confirmation that quantum interference effects in ballistic microstructures actually can be used to distinguish quasi-regular from chaotic electron dynamics. It should be noted however that these experiments are difficult and other experiments on integrable cavities with polygonal shape have failed to detect a significant deviation from the chaotic behavior [83.93].

4.11. Other aspects of chaotic ballistic transport

Another theoretical approach to chaotic ballistic transport is via random-matrix theory (RMT) [94]. This approach assumes that the junction is described by a hamiltonian from the Gaussian ensembles strongly coupled to the leads [90,95] or equivalently that the S-matrix of the junction is described by the Dyson circular ensemble [96.97]; it can calculate the amplitude and lineshape of the WL effect as well as the variance of the conductance fluctuations. This approach has no problem with unitarity to the required order and yields the value $\delta T_{WL} = 1/4$ [95–97] as well as the Lorentzian lineshape [90], in agreement with Eq. (4.21) (but without the hand-waving to get the amplitude). It also predicts conductance fluctuations with a variance $\langle(\delta T)^2\rangle = 1/8\beta$ where $\beta = 1, 2$ depending on the presence or absence of time-reversal symmetry. It cannot address at *all* the non-chaotic junctions to which the RMT ensembles do not apply.

It has now been understood [14,98,99] that although disordered microstructures are certainly classically chaotic their statistical properties differ from those predicted by the standard Wigner–Dyson ensembles. This difference comes about essentially because a disordered system is described by a *product* of random matrices [100], which leads to a different form for the eigenvalue repulsion in the S-matrix [99]. These difference are relatively small [99] when comparing the ballistic WL and UCF effects to quasi-one-dimensional disordered systems (in the metallic regime), but become greater in two and three dimensions or when strong disorder leads to localization. Thus quantum interference effects in ballistic chaotic junctions are not identical to those of disordered systems. The ballistic junctions may be regarded as the "quasi-zero-dimensional" limit of a disordered quantum conductor.

Another interesting system is the ballistic quantum dot [62,63,66] in which the electron cavities we have been discussing are separated from the leads by tunnel junctions. In this case the Coulomb charging energy [67] associated with the dot determines the spacing of conductance resonances, but we have proposed that the resonance amplitude is controlled by quantum interference effects [68]. The probability distribution for the amplitude may be calculated from standard RMT [68,101]. Recent experimental results find excellent agreement with this theory [102].

4.12. Summary

Standard transport theory has to be extended to treat mesoscopic systems since the transport coefficients depend on sample and measurement geometry and on the particular impurity configuration in the case of disordered conductors. Quantities must be studied which are meaningful for a *given* mesoscopic system and not just for the average over an ensemble. The scattering approach of Landauer, Büttiker and Imry is a powerful approach to this end. It was shown above to be rigorously equivalent to quantum linear response theory applied to an infinite system of non-interacting fermions. In the case of ballistic junctions it naturally describes both classical magnetic and geometric effects and quantum interference effects via semiclassical theory of the transmission coefficients. Theory and recent experiments on these systems indicate that it is possible to distinguish chaotic from regular electron dynamics based solely on the statistical properties of the quantum interference phenomena in transport.

Acknowledgements

I would like to acknowledge the contributions of my collaborators to the work described in these lectures. First, it has been my pleasure to collaborate with Harold Baranger who was centrally involved in almost all of the topics discussed above. Rodolfo Jalabert was a major collaborator on both the classical and semiclassical ballistic transport effects. My PhD students Jens Nöckel and Aaron Szafer made key contributions to the work on deriving the scattering approach from linear response theory. I have also enjoyed collaborations with Yoram Alhassid, Henrik Bruus, David DiVincenzo, and Matthew Hastings on some of the topics discussed. Valuable conversations are acknowledged with Markus Büttiker, Yoseph Imry, Rolf Landauer, Pier Mello and Jean-Louis Pichard. I also want to thank Peter Burke, Albert Chang, Mark Keller, Dan Prober and Sean Washburn for providing several of the figures used in the text. Much of this work was supported by NSF grants DMR-9215065,DMR-8658135.

References

[1] A.A. Abrikosov, Fundamentals of the Theory of Metals (North-Holland, 1988).

[2] E. Abrahams, P.W. Anderson, D.C. Licciardello, and T.V. Ramakrishnan, Phys. Rev. Lett. **42** (1979) 673.

[3] B.L. Al'tshuler, D.E. Khmelnitskii, A.I. Larkin, P.A. Lee, Phys. Rev. B **22** (1980) 5142.

[4] See G. Bergmann, Phys. Rep. **107** (1984) 11 for an experimental review.

[5] R.A. Webb, S. Washburn, C.P. Umbach and R.B. Laibowitz, Phys. Rev. Lett. **54** (1985) 2696.

[6] S. Washburn and R.A. Webb, Adv. Phys. 35 (1986) 375.

[7] C.P. Umbach, S. Washburn, R.B. Laibowitz and R.A. Webb, Phys. Rev. B **30** (1984) 4048.

[8] A.D. Stone, Phys. Rev. Lett. **54** (1985) 2692.

[9] P.A. Lee and A.D. Stone, Phys. Rev. Lett. **55** (1985) 1622.

[10] B.L. Altshuler, JETP Lett. **41** (1985) 648.

[11] B.L. Altshuler and D.E. Khmelnitskii, JETP Lett. **42** (1985) 359.

[12] W.J. Skocpol, P.M. Mankiewich, R.E. Howard, L.D. Jackel, D.M.Tennant and A.D. Stone, Phys. Rev. Lett. **56** (1986) 2865.

[13] P.A. Lee, A.D. Stone and H. Fukuyama, Phys. Rev. B **35** (1987) 1039.

[14] B.L. Altshuler and B.I. Shklovskii, Sov. Phys. JETP **64** (1986) 127.

[15] See the chapter by H. Bouchiat, Course 2 this volume.

[16] B.L. Altshuler. Course 1 this volume.

[17] C.P. Umbach, P. Santhanam, C. Van Haesendonck and R.A. Webb, Appl. Phys. Lett. **50** (1987) 1289.

[18] R. Webb and S. Washburn, Physics Today, **41** (1988) 53.

[19] H.U. Baranger, A.D. Stone and D.P. DiVincenzo, Phys. Rev. B **37** (1988) 6521.

[20] C.L. Kane, P.A. Lee and D.P. DiVincenzo, Phys. Rev. B **38** (1988) 2995.

[21] S. Hershfield and V. Ambegaokar, Phys. Rev. B **38** (1988) 7909.

[22] R.A. Webb, S. Washburn and C.P. Umbach, Phys. Rev. B **37** (1988) 8455.

[23] V. Chandrasekhar, D.E. Prober and P. Santhanam, Phys. Rev. Lett. **61** (1988) 2253.

[24] C.J.B. Ford, S. Washburn, M. Büttiker, C.M. Knoedler and J.M. Hong, Phys. Rev. Lett. **62** (1989) 2724.

[25] A.D. Stone and A. Szafer, IBM J. Res. Dev. **32** (1988) 384.

[26] R. Landauer, Phil. Mag. **21** (1970) 863.

[27] E.N. Economou and C.M. Soukoulis, Phys. Rev. Lett. **46** (1981) 618.

[28] D.S. Fisher and P.A. Lee, Phys. Rev. B **23** (1981) 6851.

[29] H.L. Engquist and P.W. Anderson, Phys. Rev. B **24** (1981) 1151.

[30] Y. Imry, in: *Directions in Condensed Matter Physic*, G. Grinstein and G Mazenko, eds. (World Scientific. Singapore, 1986).

[31] B.J. van Wees et al., Phys. Rev. Lett. **60** (1988) 848.

[32] D.A. Wharam et al., J. Phys. C **21** (1988) L209.

[33] M. Büttiker, Phys. Rev. Lett. **57** (1986) 1761.

[34] M. Büttiker, IBM J. Res. Dev. **32** (1988) 317.

[35] R. Spal, J. Appl. Phys. **51** (1980) 4221; H.H. Sample, W.J Bruno, S.B. Sample and E.K. Sichel, J. Appl. Phys. **61** (1987) 1079.

[36] L.I. Glazman, G.B. Lesovick, D.E. Khmelnitskii, and R.I. Shekhter, Pis'ma Ah. Teor. Fiz. **48** (1988) 218 [JETP Lett. **48** (1988) 238].

[37] A. Szafer and A.D. Stone, Phys. Rev. Lett. **62** (1989) 300.

[38] M. Büttiker Phys. Rev. B **38** (1988) 9375.

[39] A.D. Stone, and A. Szafer, P.L. McEuen and J.K. Jain, Ann. N.Y. Acad. Sci. **581** (1990) 21; and references therein.

[40] H.U. Baranger and A.D. Stone, Phys. Rev. B **40** (1989) 8169.
[41] G. Timp, A.M. Chang, P. Mankiewich, R.E. Behringer, J.E. Cunningham, T.Y. Chang and R.E. Howard, Phys. Rev. Lett. **59** (1987) 732.
[42] Y. Takagaki, K. Gamo, S. Namba, S. Ishida, S. Takaoka, K. Murase, K. Ishibashi and Y. Aoyagi. Sol. State Comm. **68** (1988) 1051.
[43] G. Timp, H.U. Baranger, P. deVegvar, J.E. Cunningham, R.E. Howard, R.E. Behringer and P. Mankiewich, Phys. Rev. Lett. **60** (1988) 2081.
[44] Landauer has frequently stated that the scattering approach taken in a more general sense can describe a wider range of systems (see e.g. R. Landauer, IBM J. Res. Dev. **32** (1988) 306) and a number of generalized "Landauer formulas" describing interacting problems have appeared in the literature. However if one wishes to maintain the key relation that each channel carries a current $e/h\Delta\mu$ (as do non-interacting fermions) it becomes necessary to assume that the transmission coefficients take on special values which have no simple interpretation.
[45] R. Kubo, J. Phys. Soc. Jpn. **12** (1957) 570; D.A. Greenwood, Proc. Phys. Soc. London **71** (1958) 585.
[46] G.D. Mahan, Many-Particle Physics (Plenum, 1981), p. 201.
[47] J.U. Nöckel, A.D. Stone and H.U. Baranger, Phys. Rev. B **48** (1993) 17569.
[48] There is a lucid elementary treatment of this in: E.M. Purcell, Electricity and Magnetism, *Berkeley Physics Course*, Vol. 2 (McGraw-Hill, 1963).
[49] A.L. Fetter and J.D. Walecka, Quantum Theory of Many-Particle Systems (McGraw-Hill, 1971), p. 298.
[50] F. Sols, Phys. Rev. Lett. **67** (1991) 2874.
[51] K. Shepard, Phys. Rev. B **43** (1991) 11623.
[52] M. Büttiker, A. Prêtre and H. Thomas, Phys. Rev. Lett. **70** (1993) 4114.
[53] C.L. Kane, R.A. Serota, and P.A. Lee, Phys. Rev. B **37** (1988) 6701. The non-local corrections to the average cancel when integrated over the sample and are normally neglected.
[54] Y. Gefen, Y. Imry and M. Ya. Azbel, Phys. Rev. Lett. **52** (1984) 129.
[55] A.D. Stone and Y. Imry, Phys. Rev. Lett. **56** (1986) 189.
[56] M.L. Roukes, A. Scherer, S.J. Allen, Jr., H.G. Craighead, R.M. Ruthen, E.D. Beebe, and J.P. Harbison, Phys. Rev. Lett. **59** (1987) 3011; M.L Roukes et al., Phys. Rev. Lett. **64** (1990) 1154.
[57] C.J.B. Ford, T.J. Thornton, R. Newbury, M. Pepper, H. Ahmed, D.C. Peacock, D.A. Ritchie, J.E.F. Frost, and G. A.C. Jones, Phys. Rev. B **38** (1988) 8518.
[58] C.J.B. Ford, S. Washburn, M. Büttiker, C.M. Knoedler, and J.M. Hong, Phys. Rev. Lett. **62** (1989) 2724.
[59] A.M. Chang, T.Y. Chang, and H.U. Baranger, Phys. Rev. Lett. **63** (1989) 1860.
[60] G. Timp, in: *Mesoscopic Phenomena in Solids*, B.L. Altshuler, P.A. Lee, and R.A. Webb, eds. (North-Holland, New York, 1991), chapter 7.
[61] R.E. Behringer, G. Timp, H.U. Baranger and J.E. Cunningham, T.Y. Chang and R.E. Howard, Phys. Rev. Lett. **66** (1991) 930.
[62] U. Meirav, M.A. Kastner and S.J. Wind, Phys. Rev. Lett. **65** (1990) 771.
[63] L.P. Kouwenhoven et al., Z. Phys. B **85** (1991) 367.
[64] C.M. Marcus, A.J. Rimberg, R.M. Westervelt, P.F. Hopkins, and A.C. Gossard, Phys. Rev. Lett. **69** (1992) 506.
[65] M.W. Keller, O. Millo, A. Mittal, D.E. Prober, and R.N. Sachs, Surf. Sci. **305** (1994) 501.
[66] P.L. McEuen, E.B. Foxman, U. Meirav, M.A. Kastner, Y. Meir, N.S. Wingreen and S.J. Wind, Phys. Rev. Lett. **66** (1991) 1926.
[67] D.V. Averin and K.K. Likharev, in: *Mesoscopic Phenomena in Solids*, B.L. Altshuler, P.A. Lee, and R.A. Webb, eds. (Elsevier, Amsterdam, 1991).
[68] R.A. Jalabert, A.D. Stone, and Y. Alhassid, Phys. Rev. Lett. **68** (1992) 3468.

[69] For reviews see M.C. Gutzwiller, Chaos in Classical and Quantum Mechanics (Springer Verlag, New York, 1991) and Chaos and Quantum Physics, M.-J. Giannoni, A. Voros, and J. Zinn-Justin, eds. (North-Holland, New York, 1991).
[70] R.A. Jalabert, H.U. Baranger, and A.D. Stone, Phys. Rev. Lett. **65** (1990) 2442.
[71] H.U. Baranger, D.P. DiVincenzo, R.A. Jalabert, and A.D. Stone, Phys. Rev. B **44** (1991) 10637.
[72] H.U. Baranger, R.A. Jalabert, and A.D. Stone, Chaos **3** (1993) 665.
[73] C.W.J. Beenakker and H. van Houten, Phys. Rev. Lett. **63** (1989) 1857.
[74] H.U. Baranger and A.D. Stone, Phys. Rev. Lett. **63** (1989) 414.
[75] C.W.J. Beenakker and H. van Houten, Phys. Rev. B **39** (1989) 10445.
[76] Y. Imry, in: *Nanostructure Physics and Fabrication*, M. A. Reed and W.P. Kirk, eds. (Academic Press, New York, 1989), p. 379; A. Yacoby and Y. Imry, Phys. Rev. B **41** (1990) 5341.
[77] That scrambling was not a factor in the quenching was perhaps unsurprising since suppression of the Hall resistance is not observed in disordered junctions where the elastic scattering surely produces scrambling.
[78] M.L. Roukes and O.L. Alerhand, Phys. Rev. Lett. **65** (1990) 1651.
[79] C.M. Marcus, R.M. Westervelt, P.F. Hopkins and A.C. Gossard, Phys. Rev. B **48** (1993) 2460; Chaos **3** (1993) 643; and Surf. Sci. **305** (1994) 480.
[80] M.J. Berry, J.H. Baskey, R.M. Westervelt and A.C. Gossard, Surf. Sci. **305** (1994) 495; M.J. Berry et al., Phys. Rev. B **50** (1994) 8857; M.J. Berry et al., Phys. Rev. B **50** (1994) 17721.
[81] A.M. Chang and H.U. Baranger, L.N. Pfeiffer and K.W. West, Phys. Rev. Lett. **73** (1994) 2111.
[82] I.H. Chan, R.M. Clarke, C.M. Marcus, K. Campman, A.C. Gossard, Phys. Rev. Lett. (1995) in press.
[83] M.W. Keller, Yale PhD thesis (1995).
[84] For a semiclassical treatment of WL in disordered systems see S. Chakravarty and A. Schmid, Phys. Rep. **140** (1986) 193.
[85] R. Jensen, Chaos **1** (1991) 101.
[86] E. Doron, U. Smilansky, and A. Frenkel, Physica D **50**, 367 (1991); Phys. Rev. Lett. **65** (1990) 3072.
[87] M.V. Berry and M. Robnik, J. Phys. A **19** (1986) 649.
[88] For more realistic treatments of the potential in GaAs microstructures see: J.A. Nixon and J.H. Davies, Phys. Rev. B **41** (1990) 7929; J.A. Nixon, J.H. Davies, and H.U. Baranger, Phys. Rev. B **43** (1990) 12638.
[89] W.A. Lin, J.B. Delos and R.V. Jensen, Chaos **3** (1993) 655.
[90] Z. Pluhar, H.A. Weidenmüller, J.A. Zuk, and C.H. Lewenkopf, Phys. Rev. Lett. **73** (1994) 2115.
[91] M.B. Hastings, A.D. Stone and H.U. Baranger, Phys. Rev. B **50** (1994) 8230.
[92] R. Blümel and U. Smilansky, Phys. Rev. Lett. **60** (1988) 477; Physica D **36** (1989) 111; Phys. Rev. Lett. **64** (1990) 241.
[93] A.M. Chang, unpublished.
[94] O. Bohigas, in reference [69]; and references therein.
[95] S. Iida, H.A. Weidenmüller, and J.A. Zuk, Phys. Rev. Lett. **64** (1990) 583 and Ann. Phys. **200** (1990) 219.
[96] H.U. Baranger and P.A. Mello, Phys. Rev. Lett. **73** (1994) 142; H.U. Baranger and P.A. Mello, Phys. Rev. B. (1995) in press.
[97] R.A. Jalabert, C.W.J. Beenakker and J.-L. Pichard, Europhys. Lett. **27** (1994) 255.
[98] N. Argaman, Y. Imry, and U. Smilansky, Phys. Rev. B **47** (1993) 4440.
[99] C.W.J. Beenakker and B. Rejaei, Phys. Rev. Lett. **71** (1993) 3689.
[100] A.D. Stone, P.A. Mello, K. Muttalib, and J.-L. Pichard, in: *Mesoscopic Phenomena in Solids*, B.L. Altshuler, P.A. Lee, and R.A. Webb, eds. (North-Holland, New York, 1991).
[101] H. Bruus and A.D. Stone, Phys. Rev. B **50** (1994) 18275.
[102] A.M. Chang et al., preprint.